In press in *The Journal of Neuroscience*, April 2019

Reduced Pre-Movement Positivity During the Stimulus-Response Interval Precedes Errors: Using Single-Trial and Regression ERPs to Understand Performance Deficits in ADHD

Scott J. Burwell[1,2], Scott Makeig[3], William G. Iacono, Stephen M. Malone[1]

1. Minnesota Center for Twin and Family Research, University of Minnesota Twin Cities, Minneapolis MN 55455
2. Department of Psychiatry, University of Minnesota Twin Cities, Minneapolis MN 55454
3. Swartz Center for Computational Neuroscience, University of California San Diego, La Jolla CA 92093-0559

Corresponding author: Scott J. Burwell, PhD
F282/2A West Building
2450 Riverside Avenue South
Minneapolis, MN 55454
Email: burwell@umn.edu

Abstract

Brain mechanisms linked to incorrect response selections made under time pressure during cognitive task performance are poorly understood, particularly in adolescents with attention-deficit hyperactivity disorder (ADHD). Using subject-specific multimodal imaging (EEG, MRI, behavior) during flanker task performance by a sample of 94 human adolescents (mean age = 15.5 years, 50% female) with varying degrees of ADHD symptomatology, we examined the degree to which amplitude features of source-resolved event-related potentials (ERPs) from brain independent component processes within a critical (but often ignored) period in the action selection process, the stimulus-response interval, were associated with motor response errors (across trials) and error rates (across individuals). Response errors were typically preceded by two smaller peaks in both trial-level and trial-averaged ERP projections from posterior medial frontal cortex (pMFC): a Frontocentral P3 peaking about 390 milliseconds after stimulus onset, and a Pre-Movement Positivity (PMP) peaking about 110 milliseconds before the motor response. Separating overlapping stimulus-locked and response-locked ERP contributions using a “regression ERP” approach showed that trial errors and participant error rates were primarily associated with smaller PMP, and not with Frontocentral P3. Moreover, smaller PMP mediated the association between larger numbers of errors and ADHD symptoms, suggesting the possible value of using PMP as an intervention target to remediate performance deficits in ADHD.

Introduction

Brain mechanisms linked to errors during cognitive task performance remain elusive, such that action monitoring research has focused on brain physiology that occurs too early (preceding the error trial by one or more trials) or too late (following the error) to enable insight into perceptual and motor processes occurring during the error trial itself. Yet, such insights may be valuable for understanding why individuals with attention-deficit hyperactivity disorder (ADHD) make many mistakes during cognitive tasks (Lijffijt, Kenemans, Verbaten, & van Engeland, 2005; Mullane, Corkum, Klein, & McLaughlin, 2009) and are also more accident prone in myriad life situations (Brook & Boaz, 2006; Jerome, Habinski, & Segal, 2006; Swensen et al., 2004; Vaa, 2014).

Functional brain antecedents to error proneness in ADHD may be considered on multiple time-scales. For instance, slowly-evolving lapses in attentional processes reflected by frontal hemodynamic deactivations (Eichele et al., 2008; Weissman, Roberts, Visscher, & Woldorff, 2006) and event-related potential (ERP) amplitude reductions (Allain, Carbonnell, Falkenstein, Burle, & Vidal, 2004; Hajcak, Nieuwenhuis, Ridderinkhof, & Simons, 2005; Masaki, Murphy, Kamijo, Yamazaki, & Sommer, 2012; O'Connell et al., 2009; Ridderinkhof, Nieuwenhuis, & Bashore, 2003) may precede errors on long time-scales (e.g., one or several trials before commencement of the error trial itself). Similar processes have accompanied errors in ADHD (Sonuga-Barke & Castellanos, 2007; Yordanova et al., 2011), suggesting diminished perceptual resources in ADHD. However, this line of research does not account for brain processes on error trials themselves, specifically within the short time-scale (≈ 0.5 second) action selection period between stimulus presentation and the motor response.

To date, the *stimulus-response interval (SRI)* with respect to errors in selective attention speeded motor response tasks remains confounded, such that it is unclear whether error-related effects during the SRI may be attributable to stimulus-evoked (perceptual) or response-preceding (motor) processes. For example, amplitudes of ERP peaks following stimulus-presentation have correlated with trial performance in some studies (Perri, Berchicci, Lucci, Spinelli, & Di Russo, 2015; Perri, Berchicci, Spinelli, & Di Russo, 2014), as have amplitudes from ERP peaks preceding motor responses in other studies (Bode & Stahl, 2014; Meckler, Carbonnell, Hasbroucq, Burle, & Vidal, 2013; Roger, Nunez Castellar, Pourtois, & Fias, 2014), but whether these separate sets of findings reflect stimulus- or response-related phenomena remains unclear. This is because the standard practice of computing ERPs by averaging voltages across trials time-locked to *either*

stimulus or response event, without accounting for possible overlap among the two processes (that often occur in rapid succession), suggests that some effect of potentials related to the response are possibly contained in the stimulus-locked ERP (e.g., Salisbury, Rutherford, Shenton, & McCarley, 2001) and vice versa.

Methodological limitations contribute to the gap in knowledge regarding SRI error-related brain dynamics in ADHD. For instance, the observation of smaller scalp-recorded N2 and P3 stimulus-locked ERP amplitude features during correct-trial "flanker" (Eriksen & Eriksen, 1974) task performance in ADHD relative to control groups is consistent with deficits in short time-scale perceptual processes (e.g., selective attention, conflict detection; Albrecht et al., 2008; Marquardt, Eichele, Lundervold, Haavik, & Eichele, 2018; McLoughlin et al., 2009), but because prior studies of this nature have largely ignored stimulus-locked ERPs on error trials, it is unknown whether such ERP features relate to erroneous performance. Additionally, prior studies in ADHD subjects have not accounted for possible overlap among stimulus and response processes, making it unclear whether ADHD-related effects reflect differences in stimulus- or response-related processing.

Here, we sought to identify stimulus- and response-locked brain potentials occurring within the SRI (between visual stimulus presentation and the button press response) that are associated with errors (within individuals) and error rates (across individuals) during a speeded response flanker task in a sample of adolescents with varying degrees of ADHD symptomatology. We limited our investigation to effective brain sources using electroencephalogram (EEG) independent component analysis decomposition and equivalent current dipole localization within models constructed from subjects' MRI head images. Additionally, to disambiguate temporal confounding among overlapping stimulus- versus response-related processes, we used a "regression-ERP" approach (Smith & Kutas, 2015a, 2015b; Woldorff, 1993) akin to methods used to disentangle event-related fMRI (Hinrichs et al., 2000) and electrodermal (Bach, Flandin, Friston, & Dolan, 2010) responses. We hypothesized that brain potentials related to errors would be associated with the increased error rate of individuals with higher levels of ADHD symptomatology in a community-based sample of adolescent youth.

Methods

Participants. Forty-eight pairs of monozygotic twins (*M* [*SD*] age = 15.5 years [.9], 50% female) were enrolled in the AdBrain study (for more information on this study, see: Burwell, Malone, & Iacono, 2016; Malone et al., 2014; Silverman et al., 2014; Wilson, Malone, Thomas, & Iacono, 2015) conducted under the auspices of the Minnesota Center for Twin and Family Research (MCTFR) at the University of Minnesota (UMN). Written informed consent was obtained from parents for their children's participation and children's written informed assent was obtained for their participation. The protocol and ethics were approved by the UMN Institutional Review Board. Diagnostic interviews and EEG recording took place at the MCTFR; neuroimaging took place on a separate day at UMN's Center for Magnetic Resonance Research (CMRR). On average, assessments at the MCTFR and CMRR were separated by 10.6 days, with 83.3% of subjects completing both within two weeks.

Lifetime symptoms of ADHD were assessed using the Diagnostic Interview for Children and Adolescents (DICA, parent and child versions; Reich, 2000), modified to include *Diagnostic and Statistical Manual of Mental Disorders* (4^{th} ed., text revision, *DSM*; American Psychiatric Association, 2000). Symptoms were assigned if endorsed by either parent or adolescent (Kosten & Rounsaville, 1992; Leckman, Sholomskas, Thompson, Belanger, & Weissman, 1982). The presence of diagnosable ADHD in this community sample was substantial (12.5%), with participants on average possessing between two and three ADHD symptoms (*M* [*SD*] = 2.6 [3.9]).

Electrophysiological assessment

Flanker task. Subjects were seated in a comfortable chair in a sound attenuated, dimly lit room. An index finger response button was positioned on each armrest. Subjects performed a modified version of the flanker task (Eriksen & Eriksen, 1974). Task stimuli consisted of five-character arrays of the letters *S* and *H*. Four such target arrays appeared on screen in pseudo-random order with the following relative frequencies: *SSSSS* (33.3%); *HHHHH* (33.3%); *SSHSS* (16.7%); and *HHSHH* (16.7%). In each array, the target stimulus was the central character, which determined the desired subject response (button press); the other four characters (*S* or *H* "flankers") had no relevance to the intended response. On each trial, the target and flanker characters were presented simultaneously at the center of a computer screen facing the subject. Before the task training block (*N* trials = 20), subjects were instructed to indicate by pressing the left-button that the target stimulus was an *S,* and to indicate with a right-button press that the target stimulus was an *H*, and that these hand-to-letter assignments would vary across subsequent task blocks. Each array was presented for 100 ms. Stimulus presentations were separated by a mean of 2190 ms (*SD* = 60), varying pseudo-randomly across trials in the range 2000 to 2300 ms. Valid responses were only recorded when the subject responded within 1150 ms following stimulus onset.

Subjects were instructed to respond as quickly and accurately as possible; we checked their performance in the training block prior to beginning the EEG recording to ensure that they understood the task.

EEG was recorded during three blocks of 150 trials. Target-stimulus hand mapping was alternated in successive blocks: Block 1 (*S* = right, *H* = left), Block 2 (*S* = left, *H* = right), and Block 3 (*S* = right, *H* = left). Trials in which central and flanker stimuli were the same (e.g., central = *S*, flanker = *S*) were termed "congruent" stimulus trials; trials in which central and flanker stimuli were not the same (e.g., central = *S*, flanker = *H*) were termed "incongruent" stimulus trials.

Data for 10 task blocks in which response accuracy fell below chance (e.g., because of incorrect hand mapping during the block) were discarded. Following this process, one subject was excluded because his overall error rate (percentage of incorrectly performed responses) exceeded 40%. Two additional subjects were excluded because EEG data were contaminated with non-brain artifact, leaving 93 subjects for remaining analyses.

EEG recording and processing. EEG data were recorded continuously during performance of the flanker task (61 scalp electrodes; a 10/10 System electrode cap; 1024 Hz sample rate; pass-band, DC to 205 Hz) with a BioSemi ActiveTwo system (BioSemi, Amsterdam, Netherlands). Eye-movement related contributions to the EEG signals were monitored using a pair of electrodes placed above and below the right eye and another pair of electrodes placed on left and right temples. A common recording reference was used for EEG and eye-movement channels. Custom MATLAB (The MathWorks Inc., Natick, MA) scripts using functions from the EEGLAB software environment (Delorme & Makeig, 2004) were used for removing artifact-contaminated time-segments and channels by a method previously described (available for download at *github.com/sjburwell/eeg_commander*; Burwell, Malone, Bernat, & Iacono, 2014; Burwell et al., 2016). Artifact-cleaned data were down sampled to 256 Hz, high-pass filtered above 0.1 Hz, and re-referenced at each time point to the average potential of all the channels.

Subject EEG source separation, dipole localization, and inter-subject co-registration. Scalp-recorded EEG data channels contain a spatiotemporal mixture of multiple brain and non-brain source activities. To "un-mix" putative brain sources from other brain and non-brain sources whose volume-conducted potentials were summed in the scalp electrode signals, we decomposed each subject's continuous EEG using Adaptive Mixture Independent Component Analysis (AMICA; Delorme, Palmer, Onton, Oostenveld, & Makeig, 2012; J. Palmer, Kreutz-Delgado, & Makeig, 2006; J. A. Palmer, Kreutz-Delgado, Rao, & Makeig, 2007) to obtain effective EEG source activities that exhibit maximal temporal independence (see **Figure 1A** and **B**). Low-frequency (< 1.0 Hz) drifts in EEG, in some cases reflecting sweat or electrode artifacts, often account for much variance in the data and may introduce spatiotemporal non-stationarity, which

tends to adversely impact ICA decompositions (Debener, Thorne, Schneider, & Viola, 2010). Therefore, AMICA models were trained on data that was high-pass filtered above 1.0 Hz. For ERP analyses the resultant ICA decomposition was applied to the 0.1-Hz high-pass filtered data (Debener et al., 2010; Winkler, Debener, Muller, & Tangermann, 2015). Channel weights (W^{-1} in **Figure 1B**) for each effective source (independent component) were then used for subsequent dipole localization.

For subject-specific dipole localization, MRI T1-weighted anatomical images were acquired from each subject using a 3-T Tim Trio scanner (Siemens Medical Systems, Erlangen, Germany) and a magnetization prepared rapid gradient echo (MPRAGE) sequence (TR = 2530 ms, TE = 3.65 ms, flip angle 7°, matrix size = 256 x 256 with a FOV of 256, 240 sagittal slices with 1-mm^3 isomorphic voxels). Using the Neuroelectromagnetic Forward Head Modeling Toolbox (NFT; Acar & Makeig, 2010), a realistic boundary-element method (BEM) head model consisting of roughly 7,000 nodes for each layer of scalp, skull, cerebrospinal fluid (CSF), and brain mesh was generated from the anatomical image; electrode locations were spatially registered (see **Figure 1C**) with scalp surface by aligning fiducials with nasion (midline depression between the eyes on the bridge of the nose) and two pre-auricular points (anterior region of the left and right tragus). The forward model estimation (which maps the amplitude of each dipole in source-space to the potential at each scalp-positioned channel) used recommended conductivity values for scalp (.33 Siemens [S]/meter [m]; Geddes & Baker, 1967), skull (25:1 brain-to-skull ratio, or .0132 S/m; Akalin Acar & Makeig, 2013; Lai et al., 2005), CSF (1.79 S/m; Baumann, Wozny, Kelly, & Meno, 1997), and brain (.33 S/m; Geddes & Baker, 1967) tissues. Finally, the computed forward model and scalp topography for each EEG source were used to estimate the location of a single equivalent dipole model for each source (**Figure 1D**).

To co-register dipoles across subjects, alignment parameters (**Figure 1E**) mapping each subject's brain volume into Montreal Neurological Institute (MNI) space were estimated using the AFNI program *@auto_tlrc* (Cox, 1996). Then, parameters were applied to dipole locations, resulting in all subjects' source dipoles having a common anatomical reference (see **Figure 1F**).

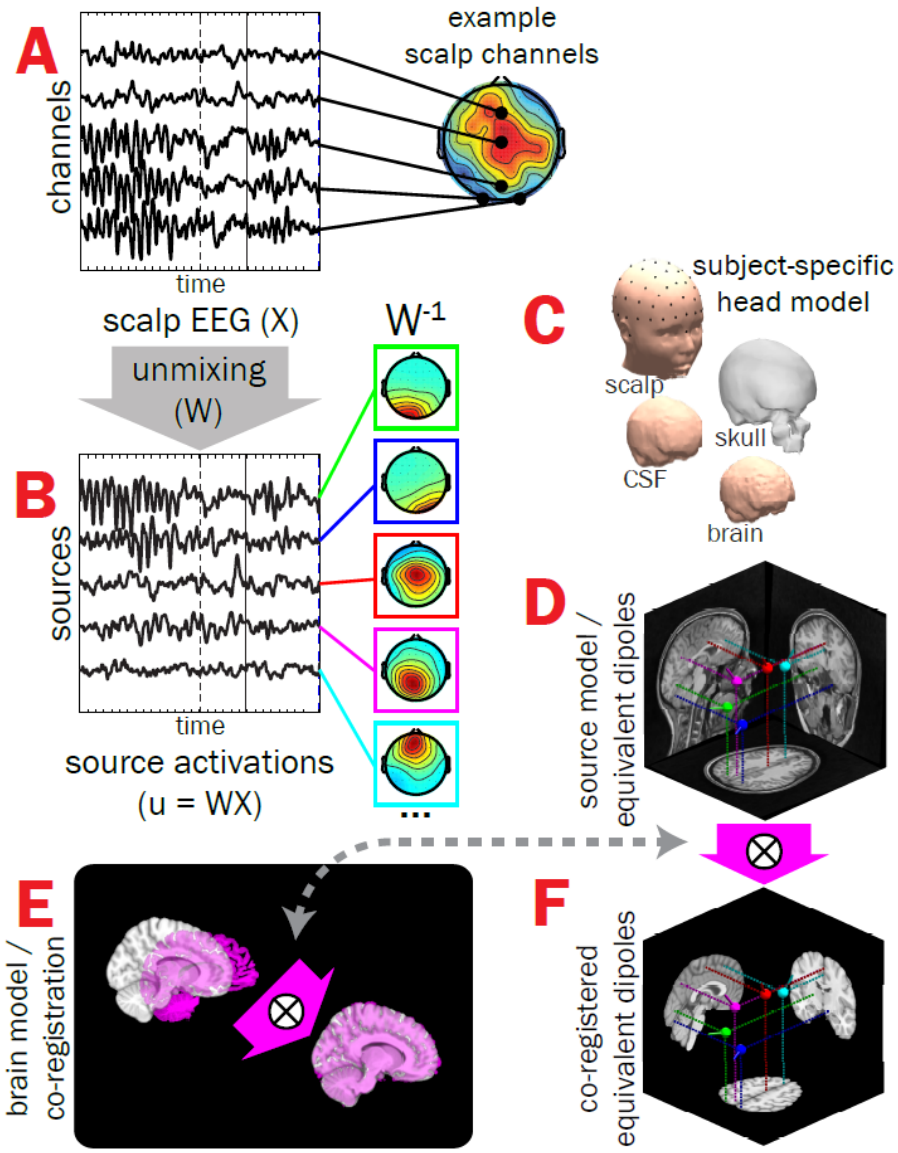

Figure 1. Subject EEG effective source separation, dipole localization, and inter-subject co-registration. A) Time-varying EEG recorded from a subset of scalp-positioned channels are plotted for a single subject during one correctly-performed trial of the flanker task (stimulus-onset = dashed vertical line, button-press = solid vertical line); note that scalp EEG for a given channel is a spatiotemporal admixture of activities from multiple brain and non-brain sources, leading to multiple "hot spots" in scalp projections. B) Adaptive Mixture Independent Component Analysis (AMICA) was used to "unmix" scalp-recorded channel data (by finding the un-mixing matrix, W) into putative EEG effective "source" signals with maximal temporal independence (only a subset shown here on the left) and associated scalp topographies (middle, W^{-1}). C) Subject-specific head models created from structural MRIs were then used with scalp topographies to estimate the coordinates of each source's equivalent current dipole (D). E) Finally, alignment parameters mapping a given subject's brain volume (magenta) onto the MNI template brain (gray) were obtained and applied to dipole coordinates, resulting in all subjects' source model dipoles having a common neuroanatomical reference (F). X = scalp-recorded EEG (channels-by-time); W = unmixing matrix derived from ICA; u = EEG effective source activations (sources-by-time); W^{-1} = mixing matrix (component scalp topographies).

Clustering of EEG sources across subjects. The 1,521 sources with "near-dipolar" projections (having less than 15% residual variance between dipole projection and scalp topography; see Delorme et al., 2012; McLoughlin, Palmer, Rijsdijk, & Makeig, 2013) and having coordinates within the boundaries of the template brain were grouped across subjects using EEGLAB's k-means clustering framework (Onton, Westerfield, Townsend, & Makeig, 2006). Sixteen source clusters (i.e., $round\left(\frac{total\ \#\ sources}{\#\ subjects}\right)$; Rapela et al., 2012) were determined using the following features extracted from each source as contributing factors to the k-means algorithm: the MNI coordinates of equivalent current dipole locations, four principal components from normalized continuous EEG power spectra (chosen by each having accounted for more than 5% of the total variance in within normalized spectral power), and sixteen principal components (chosen to be equal to the selected number of clusters) from scalp topographical maps. To compensate for the low dimensionality inherent to dipole coordinates and increase their influence on the k-means solution, clustering dimensions corresponding to dipole coordinates were multiplied by a factor of five (cf. Gramann et al., 2010; Piazza et al., 2016; Rapela et al., 2012).

To keep clusters homogenous in terms of their contributing factors (i.e., dipole locations, power spectra, scalp topographies), sources located more than 2 standard deviations away from each cluster centroid in k-means measure space were removed from initial clusters. While this "robust" k-means process has been shown to return homogenous clusters (e.g., Behmer & Fournier, 2016; Ehinger et al., 2014; Knaepen et al., 2015; Lisi & Morimoto, 2015), it frequently returns clusters that are missing sources from one or more subjects. Therefore, to preserve sample size, comparable sources were added from subjects having "outlying" (i.e., > 2 std. dev.) sources in the k-means output (e.g., as in McLoughlin et al., 2013) to clusters of interest (i.e., those clusters associated with errors in the stimulus-response interval) based on having smallest Euclidean distances to centroids in the clustering space.

Source activity time-series for each subject were forward projected (i.e., $X_{channel} = W^{-1}u_{source}$; see **Figure 1**) to the scalp location to which it projected most strongly across the cluster. For each source time-series, the electrical potential at each latency was then standardized as ratio to its baseline root mean-square deviation across the -800 to -300 ms pre-stimulus intervals in all trials (cf. McLoughlin et al., 2013).

Trial-level EEG measures. Error trials were matched within subject to a subset of correct trials of the same stimulus type and nearest RT, giving a set of 4,196 trials (45.0% incongruent; *n* = 91 subjects, two subjects made no errors) for trial-level EEG / error analyses. This matching procedure was important to ensure that the relative duration and timing among stimulus- and response-related brain processes for a given error response trial and its comparison correct trial

were similar; failure to adjust for variation in the duration of these processes may confound interpretation of associations between trial brain potentials and performance.

Standard trial-average ERP and "regression-ERP" (rERP) measures

Standard trial-averaged ERPs. Stimulus- and response-locked brain potentials were separately computed by the "standard" ERP approach, which averages the potential across trials at each latency relative to stimulus or response events, being largely sensitive to voltages of relatively consistent polarity at one or more latencies across trials. Standard ERPs for the four stimulus/response type combinations were averaged separately within subject. For comparability with other papers on action monitoring ERPs in youth (e.g., Anokhin & Golosheykin, 2015; Meyer, Bress, & Proudfit, 2014; Pontifex et al., 2011; Pontifex, Saliba, Raine, Picchietti, & Hillman, 2013; Torpey, Hajcak, Kim, Kujawa, & Klein, 2012), subjects were included if they possessed at least six artifact-free trials within a given stimulus/response type. As such, subject and trial counts for the four types were as follows: correct congruent (n = 93 subjects, M [SD] = 249.5 [53.2] trials), correct incongruent (n = 93 subjects, M [SD] = 119.7 [27.9] trials), error congruent (n = 63 subjects, M [SD] = 17.1 [11.7] trials), and error incongruent (n = 53 subjects, M [SD] = 15.6 [9.7] trials).

Overlap-corrected rERPs. When the time between stimulus and response varies across trials, standard ERPs "smear" overlapping stimulus- and response-locked brain potentials, such that some effect of potentials elicited by the stimulus are contained in the response-locked ERP and vice versa. Thus, "smearing" unsatisfyingly interjects uncertainty into interpretation of stimulus- versus response-related waveform features (Salisbury et al., 2001; Woldorff, 1993), making it difficult to identify potentials unique to *either* stimulus *or* response. While ICA is used here to unmix spatial blending of projections from distinct effective EEG sources to the scalp channels, it is not intended to address temporal overlapping within each EEG source time-series that are preferentially time-locked to stimulus presentations or button response events. So, an alternative to standard ERP averaging, here applied to brain source activity time series identified by ICA, is to decompose dissociable stimulus- and response-locked brain potentials via the "regression-ERP" (or rERP) framework (see methods papers by Burns, Bigdely-Shamlo, Smith, Kreutz-Delgado, & Makeig, 2013; Ehinger & Dimigen, 2018; Smith, 2011; Smith & Kutas, 2015a, 2015b), an overlap-correction approach (Woldorff, 1993) akin to deconvolution methods used in event-related fMRI (Hinrichs et al., 2000) and electrodermal (Bach et al., 2010) research that enables insight into what distinct stimulus- and response-locked processes contribute to standard ERPs in which these two processes are confounded.

In simplest terms, the rERP can be described as a vector of β coefficients from a series of regressions conducted *separately at each latency* within an epoch relative to an event. As

detailed by Smith and Kutas (2015a, b) the standard ERP is a special case of the rERP where in the model

$$y_{ij} = \beta_j X_{ij} + \varepsilon_{ij}$$

the observed EEG data y on trial i at latency j relative to a task event (e.g., stimulus onset) is the result of the "true" ERP β_j summed with un-modeled zero-mean "noise" ε at that latency; here, the trial design column matrix X consist entirely of ones with length equal to the number of trials. Equivalently, rather than conducting separate regressions sequentially at each latency j within the event-locked epoch of length J, the many regressions can be combined into a single model to estimate all $\beta_{1,2,\ldots,J}$ simultaneously (software for applying the rERP technique outlined by Smith and Kutas (2015a,b) can be found at: *github.com/sjburwell/rerp*, *vorpus.org/rERP*, *sccn.ucsd.edu/wiki/EEGLAB/RERP,* and *unfoldtoolbox.org*). Specifically, the above column matrix X may be expanded with zeros to generate an L-by-J matrix $STIM$ that accounts for all latencies L in the continuous EEG time-series (see **Figure 2A**). Here, $STIM_{i_{lj}}$ takes the value of 1 when there is intersection between the conditions of l and j (e.g., 300 ms post-stimulus in the continuous EEG on trial i *and* 300 ms post-stimulus in the event-related epoch), and 0 otherwise.

Overlap in stimulus- and response-locked brain potentials may then be modeled by horizontal concatenation of the above design matrix $STIM$ with a similar design matrix $RESP$ that is conditioned to button response events (see **Figure 2B**). For example, in the equation

$$y_{i_l} = \beta_{STIM_{300ms}} STIM_{i_{300ms}} + \beta_{RESP_{-50ms}} RESP_{i_{-50ms}} + \varepsilon_{i_l}$$

$\beta_{STIM_{300ms}}$ and $\beta_{RESP_{-50ms}}$ are "true" potentials co-occurring 300 ms after stimulus presentation and 50 ms before the button response (respectively) on trial i. As trial response times (RTs) vary, so will non-zero elements of $STIM$ and $RESP$, enabling overlap-correction.

Note that simply regressing stimulus-locked trial potentials onto a variable such as RT that encodes the temporal separation between stimulus and response events (or vice versa) is not the same as overlap-correction. Regressing trial potentials onto RT (e.g., Cohen & Cavanagh, 2011; Rousselet et al., 2009) weighs potentials from short-RT trials (i.e., high overlap) differently than potentials from long-RT trials (low overlap) in summation of "RT-regressed ERPs" but the assignment of such weights is arbitrary. Specifically, it is unclear the weight value to assign to trials where there is total overlap (i.e., simultaneous or near-simultaneous stimulus and response events) versus no overlap, resulting in ambiguous translation between RT-regressed ERPs and trial-level / trial-averaged potentials. By contrast, the overlap-corrected rERP approach that we used here *explicitly models overlap at each latency in the continuous EEG*, enabling straightforward translation between overlap-corrected rERPs and trial-level / trial-averaged potentials.

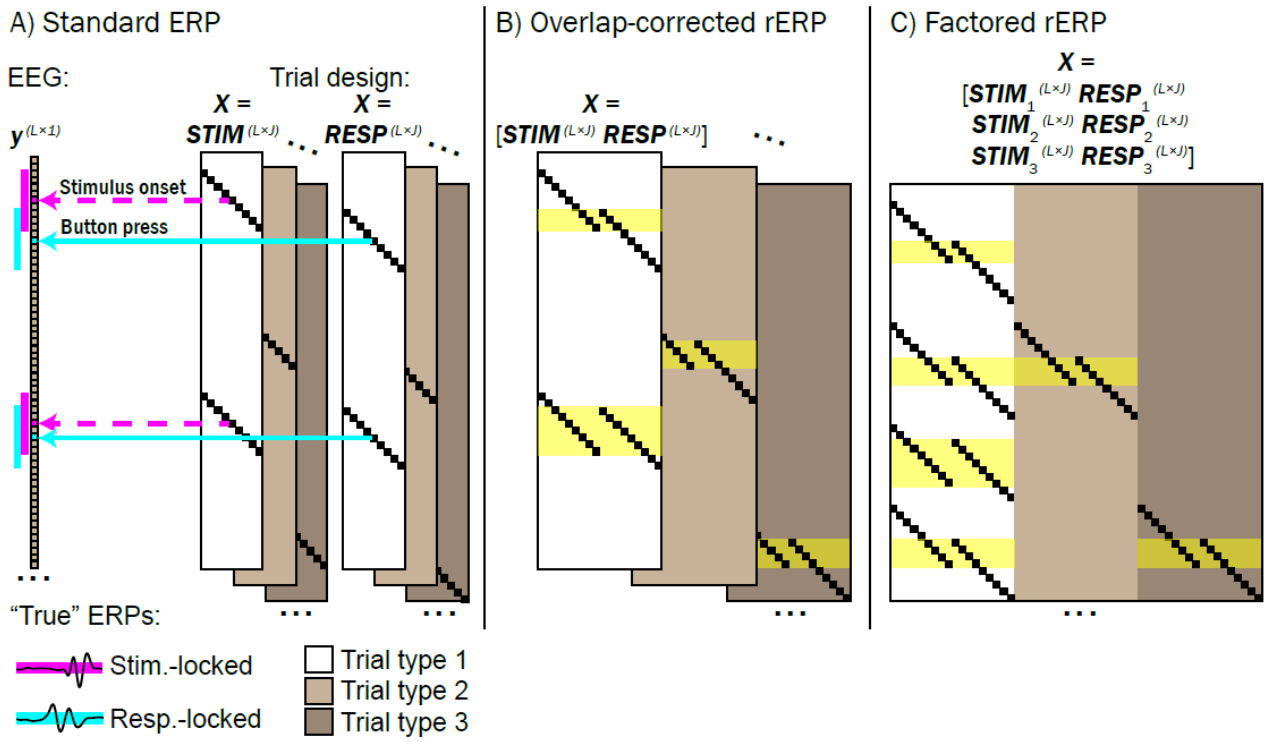

Figure 2. Comparison between standard trial-averaged ERP, overlap-corrected regression-ERP (rERP), and overlap-corrected factored rERP, using regression design. A) Standard ERPs time-locked to stimulus onset and button response events may be calculated separately by using separate $STIM$ and $RESP$ matrices substituted for the trial design matrix X, separately across different trial types (e.g., congruent correct, incongruent correct, congruent error, etc.). Here, each row of X corresponds to each latency L in the continuous EEG recording y, and each column of X corresponds to each latency within the chosen epoch for which the ERP is to be calculated (e.g., 2 seconds before and after each stimulus or response event) of length J. An element of X takes the value of 1 (small black squares) if it corresponds to a latency within the event-related epoch on a given trial number of a given trial type, and 0 otherwise. As trial RTs vary, so do overlapping non-zero elements of $STIM$ and $RESP$. Note that the standard ERP does not account for temporal overlap among stimulus and response epochs (see magenta and cyan demarcations alongside the EEG recording y), and therefore stimulus- and response-locked standard ERPs are temporally confounded. B) Overlap-correction among stimulus and response processes is achieved by horizontal concatenation of $STIM$ and $RESP$ into a single matrix X for each trial type. Here, periods within the continuous EEG recording where stimulus- and response-locked epochs overlap are highlighted in yellow. C) Concatenating task design matrices from multiple trial types may be used to explore processes that are unique to a given trial type. Using trial type 1 (white block of X) as the reference type in a treatment coding framework, the degree to which waveforms deviate from trial type 1 as a function of trial type 2 (light gray) or trial type 3 (dark gray) may be explored. For example, in our study we used congruent correct trials as the reference type (white block) and explored how rERPs deviated as a function of incongruent flanker stimuli (light gray) or errors (dark gray).

Mirroring the approach taken for standard ERPs, overlap-corrected rERPs were computed for the four stimulus/response combinations. Overlap-corrected rERPs enabled straightforward interpretation of separate stimulus- versus response-related processes, such that they provide

an estimate of what overlapping stimulus- and response-locked brain potentials separately contribute to single-trial and trial-averaged ERPs.

Overlap-corrected, factored rERPs. Taking our rERP investigation further, we used a treatment coding approach (cf. Smith and Kutas, 2015a, b) to highlight brain potentials associated with stimulus and response "factors." This strategy is similar to calculating "difference waves" (cf. Luck, 2005), whereby a standard waveform of one or more stimulus/response combinations (e.g., correct trials) may be subtracted from another (e.g., error trials), although the key advantage to factored rERPs is that they permit overlap-correction. Subtraction of scalp-recorded channel waveforms from different task conditions may distort true brain activity because the spatiotemporal sum of active sources projecting to a scalp channel at one task moment may differ from that during other moments (e.g., see discussion in Burwell et al., 2016, p. 1003). We believe the approach of using ICA-unmixed component processes can circumvent these concerns when contrasts are computed on spatially-filtered EEG *source activities* themselves.

To isolate stimulus- and response-locked rERP task factors (see **Figure 2C**), we extended the above rERP model to:

$$y_{i_l} = \beta_{STIM_{300ms}} STIM_{i_{300ms}} + \beta_{RESP_{-50ms}} RESP_{i_{-50ms}}$$
$$+\beta_{INCGRTSTIM} INCRGTSTIM_{i_{300ms}} + \beta_{INCGRTRESP} INCRGTRESP_{i_{-50ms}}$$
$$+\beta_{ERRSTIM} ERRSTIM_{i_{300ms}} + \beta_{ERRRESP} ERRRESP_{i_{-50ms}} + \varepsilon_{i_l}$$

As before, β_{STIM} and β_{RESP} reflect respective stimulus- and response-locked rERPs, but here they are fixed to a chosen reference, which we coded to be congruent correct trials. Then, in the full system of equations, $INCGRTSTIM_{i.}$ / $INCGRTRESP_{i.}$ and $ERRSTIM_{i.}$ / $ERRRESP_{i.}$ are coded 0 (for congruent trials and correct responses, respectively) and 1 (for incongruent trials and error responses, respectively). Critically, the resulting waveforms comprised by $\beta_{INCGRTSTIM,ERRSTIM}$ and $\beta_{INCGRTRESP,ERRRESP}$ do not reflect trial waveforms, but rather the expected time-varying *deviations* from waveforms β_{STIM} and β_{RESP} as a function of task stimulus and response type. We derived three stimulus-locked and three response-locked waveforms for each subject to reflect: 1) the expected brain potential for correctly-performed congruent stimulus trials, 2) the deviation time series when flanking stimuli are incongruent with the target stimulus, and 3) the deviation time series associated with making an erroneous response. We explored an incongruence-by-error interaction, but determined its impact was nonsignificant; thus, here we only report main effects of stimulus incongruence and response errors.

Statistical Analyses

Within-subject error associations using EEG, ERP, and rERP. Voltages from trial-level EEG, standard trial-averaged ERPs, and overlap-corrected rERPs were used as predictors of response errors (separately for congruent and incongruent trial types). Because data were inherently nested (i.e., trials within individual, twin within twin-pair), a multilevel model (MLM) approach was used. In the following MLM logistic regression (Pinheiro & Bates, 2000): $ERROR_{ijk} = B_{INT} + B_{ERROR}VOLTAGE_{ijk} + \alpha_{jk} + \alpha_k + \varepsilon_{ijk}$. Here, $ERROR_{ijk}$ and $VOLTAGE_{ijk}$ respectively reflect response errors (1 = error, 0 = correct) and voltages (from baseline-subtracted trial-level EEG, trial-averaged ERP, or overlap-corrected rERP) on trial type i for participant j of family k, B_{INT} is the model intercept, ε_{ijk} is random noise, and random intercept terms α_{jk} and α_k account for multiple records per subject (i.e., trials) and multiple records per family (i.e., twins), respectively.

For trial-level EEG, logistic regressions were conducted at each latency relative to stimulus or response events; for trial-averaged standard ERPs and overlap-corrected rERPs, logistic regressions were conducted for mean potentials extracted from [±50 ms] windows centered around peaks identified as relevant for errors in trial-level analyses. The reported fixed-effect coefficient B_{ERROR} reflects the expected change in probability (log odds) of an error with one standard deviation positive-going change in EEG, ERP, or rERP. Odds ratios (*OR*s, presented in tables and calculated by $\exp[B_{ERROR}]$) reflect the proportion increase in the odds of an error, adjusted for nuisance covariates (Agresti, 2013).

P-values for logistic regressions were determined by calculating the z-values for each B_{ERROR} coefficient (i.e., $\frac{B_{ERROR}}{std.error}$) and referring it to the standard normal quantile function. For significance testing of within-subject analyses (logistic regression associations with errors) we used a false discovery rate-corrected (FDR, Benjamini & Hochberg, 1995) alpha of .01; between-subjects analyses (linear regression associations with individual differences in error rate, ADHD analyses) adopted a more sensitive FDR-corrected alpha of .05, which were flagged in tables using asterisks. Although not shown in the model and not reported, trial-level or trial-averaged RT, subjects' age, and gender were included as fixed-effect nuisance covariates.

Source clusters whose trial potentials within the SRI were found significantly associated with errors across both congruent and incongruent trial types were further examined next to lateralized readiness potentials (LRPs), which are thought to reflect activation of motor preparation and execution processes and indicate the responding hand by stronger contralateral than ipsilateral hemisphere negativity (Smulders & Miller, 2011). This enabled comparing the temporal sequencing between brain processes generally related to errors and processes reflecting motor activation of the correct or erroneous button response; whichever began first may be considered be more central to error commissions. As above, MLM logistic regression

associations with errors were calculated at each latency, but instead of analyzing separately within congruent and incongruent trials, analyses were conducted separately within trials grouped by the correct-response hand (including a stimulus congruency interaction term). LRPs were calculated in the typical fashion (de Jong, Wierda, Mulder, & Mulder, 1988; Gratton, Coles, Sirevaag, Eriksen, & Donchin, 1988) by subtracting the ipsilateral scalp waveform (e.g., CP4 for right-hand responses) from that of the contralateral scalp waveform (CP3 for right-hand responses), but unlike most prior investigations studying LRPs, scalp voltages were summed projections only from independent component source clusters in or near left and right sensorimotor cortex (thereby spatially filtering out influences from other sources). We compared the relative timings of error-related effects (p_{FDR} < .01) for in LRPs alongside the other trial potentials to understand which effects manifested first.

Between-subject error rate associations using factored rERPs. We next sought to understand whether brain potentials reflected in factored rERP waveforms were associated with individual differences in task error rates (i.e., $100 * \frac{\#\ errors}{total\ \#\ of\ responses}$). Error rates for the overall sample were positively skewed, so to approximate a normal distribution to be used in linear regressions, error rates x were transformed by $\log(x + 1)$. Next, at each latency within the factored rERPs, the following MLM was estimated: $PCTERR_{ijk} = B_{INT} + B_{PCTERR}VOLTAGE_{jk} + \alpha_{jk} + \alpha_k + \varepsilon_{jk}$. In this equation, $PCTERR_{jk}$ and $VOLTAGE_{jk}$ reflect error rate and baseline-subtracted potential at a given latency relative to either stimulus or response for subject j of family k.

Do amplitude differences in rERPs mediate the association between ADHD symptom count and heightened task error rates? Possible brain mechanism(s) responsible for the association between ADHD and high task error rates remain unknown. Given an association between brain potentials and error rates, brain potentials may plausibly be tested as indicators of the relationship among ADHD symptom count and error rates. Specifically, in the mediation framework (for review, see Shrout & Bolger, 2002): *Does the predictor (ADHD symptom count) exert its statistical effect on the outcome (error rate) by way of a mediator (brain potential measure), such that when both predictor and mediator are included as covariates, the effect of the predictor variable is significantly reduced?*

We first examined whether ADHD symptom count, stimulus congruence (incongruent vs. congruent), and congruence × ADHD symptom count interaction significantly (p < .05) were associated with task error rates in MLMs (including age and gender as fixed-effect covariates and a random intercept to account for multiple records per family). In mediation framework, the main effect of ADHD on error rates may be thought of as the "total" effect, as illustrated by path *c* in **Figure 3A**. However, the "total" effect of ADHD on error rate may be partitioned into "direct" (path *c'*, **Figure 3B**) and "indirect" effects (paths *a* and *b*). The direct effect *c'* reflects the

reduction from the total effect to the indirect effect, which is mathematically equivalent to the product of *a* and *b*.

In the mediation model, a brain potential is said to have partially mediated the relationship between ADHD symptom count and error rates if the shrinkage in the value of *c* to *c'* is significant; or equivalently, if the size of the indirect effect *ab* is significantly different than zero. To quantify paths *a* and *b*, for each subject we extracted mean potentials within time segments of the factored rERP waveforms that: (1) were strongly associated with overall task error rate (requiring $p_{FDR} < .05$ for a duration of at least 50 consecutive ms in the rERP waveform), and (2) overlapped temporally with EEG/ERP time windows determined by above analyses to be robustly associated with response errors. These measures were separately tested as mediators (cf. "Brain Potential" in **Figure 3B**) in the association between ADHD symptoms and task error rates. Paths *a*, *b*, *c*, and *c'* were presented as *t*-statistics (i.e., $\frac{coeff.}{std.error}$), and denominator degrees of freedom were calculated using Kenward-Roger approximation (Kuznetsova, Brockhoff, & Bojesen Christensen, 2016).

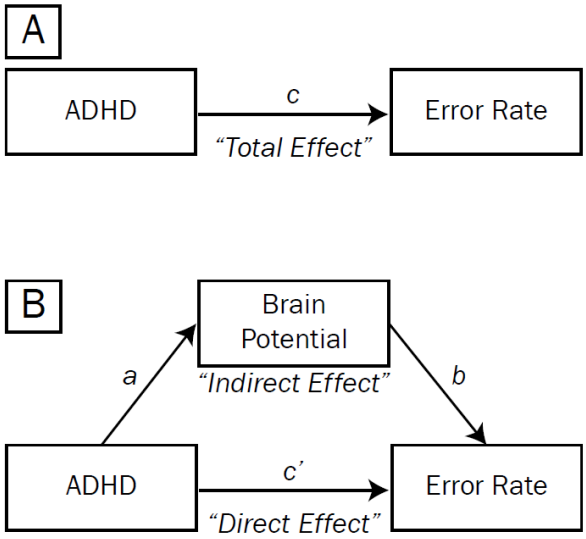

Figure 3. Mediation model testing whether brain potentials account for the association between ADHD symptom count and task error rates. The main effect of ADHD symptoms on error rates may be thought of as the "total effect", as illustrated by path *c* (A). However, the "total" effect of ADHD on accuracy may be partitioned into "direct" (path *c'*, B) and "indirect" effects (paths *a* and *b*). The direct effect *c'* reflects the reduction from the total effect to the indirect effect, which is mathematically equivalent to the product of *a* and *b*.

To estimate whether mediation was significant, we used a bootstrapping approach used by Burwell et al. (2014) whereby 1,000 indirect effects (*ab*, equivalent to the change in *c* to *c'*) were simulated from the observed data with replacement (Shrout & Bolger, 2002), keeping the proportion of matched- to unmatched-twin-pairs constant. Ninety-five percent confidence

intervals were estimated from this distribution of simulated *ab* effects to evaluate statistical significance at the .05 level; significant mediation is said to have occurred when the confidence interval did not include 0.

Results

RT associations with stimulus congruency and response accuracy. Across all subjects and trials, RTs were shorter on error trials (congruent *M* [*SD*] = 450.4 [192.6] ms, incongruent *M* [*SD*] = 438.4 [171.8] ms) than on correct trials (congruent *M* [*SD*] = 513.4 [143.5] ms, incongruent *M* = 563.0 [146.2] ms) by about 58 ms (t[36,350] = -14.63, $p < .001$, MLM linear regression); RTs were also longer on incongruent trials (main effect of incongruent stimulus, t[36,332] = 32.46, $p < .001$), and there was a significant incongruent stimulus × error response interaction (t[36,335] = -7.76, $p < .001$).

Error associations within-subject using trial-level source potentials. The subset of correct and error trials selected for trial-level EEG source analyses did not differ with respect to RT (t[4,103] = -.72, $p = .470$, MLM linear regression) and the interaction with stimulus incongruency was nonsignificant (t[4,103] = -.34, $p = .731$), confirming that the RT-matching procedure for trial-level analyses was successful and that the relative timing among stimulus- and response-related processes for a given pair of correct and error trials within subject was similar.

Error associations across source clusters. In **Figure 4**, we plotted grand mean waveforms for each trial type derived from fifteen source clusters (one cluster not shown because it corresponded to non-brain eye blink artifacts) as well as mean dipole locations. Horizontal bars plotted above waveforms highlight periods when the source electrical potential derived from individual trials was significantly associated with error responses within congruent or incongruent stimulus trials ($p_{FDR} < .01$ for a period of 50 ms or longer, MLM logistic regression). Several well-documented (e.g., Luu, Tucker, & Makeig, 2004; Overbeek, Nieuwenhuis, & Ridderinkhof, 2005; Ridderinkhof, Ullsperger, Crone, & Nieuwenhuis, 2004; Wessel, 2012) error-related effects were detected, such as stronger post-error negativity (approximately 0 to 100 ms post-response in medial frontal clusters [e.g., posterior medial frontal cortex, pMFC]) and stronger post-error positivity (approximately 100 to 600 ms post-response in pMFC and parieto-occipital clusters [e.g., POC and pPOC]) in response-locked waveforms.

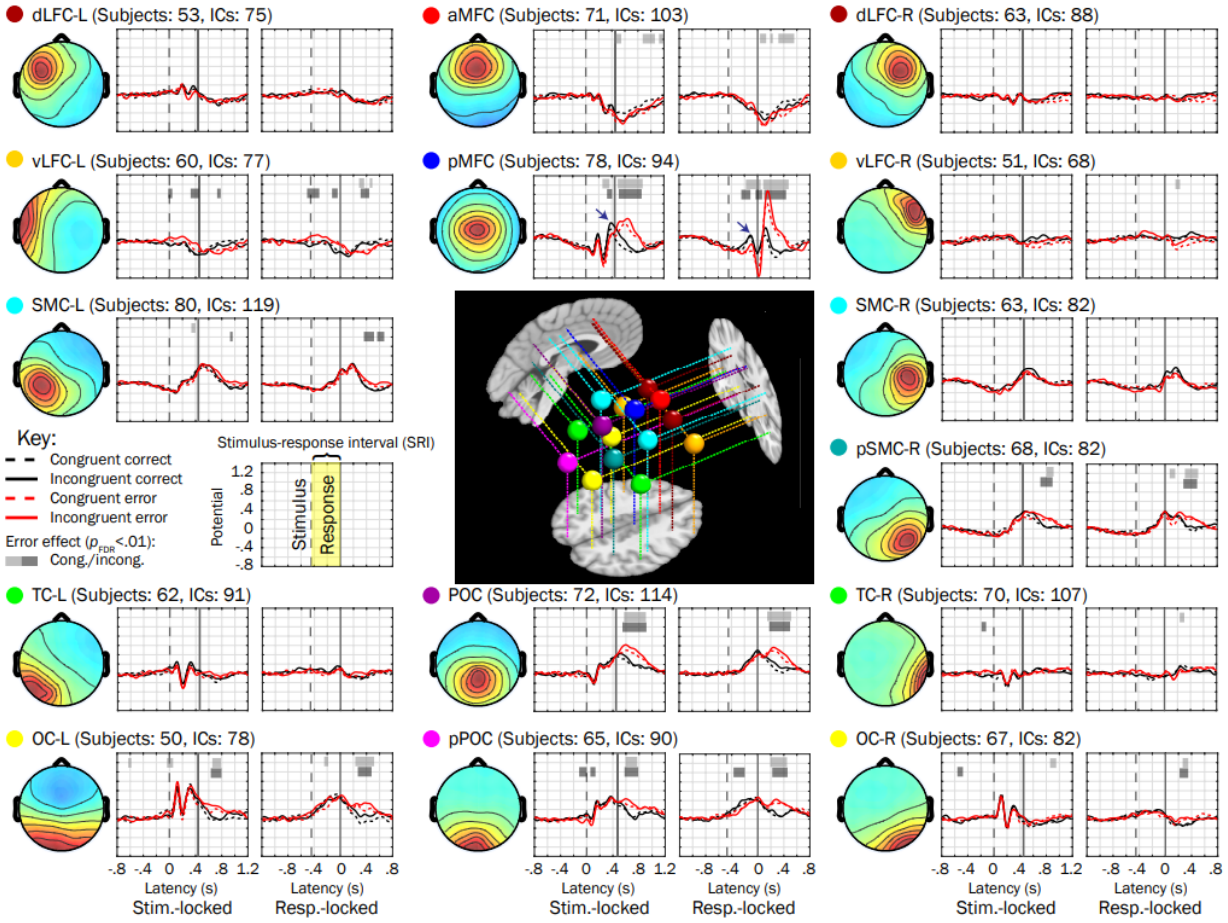

Figure 4. Fifteen source clusters, grand mean trial waveforms, and voltage associations with errors. Grand mean waveforms from error (red traces) and correct (black traces) performance trials (matched within stimulus congruency types [congruent = dashed, incongruent = solid] by response time) are plotted next to mean scalp topographies for each of 15 source clusters (one of the clusters not shown because it primarily reflected ocular activity) examined in the present study. Horizontal bars plotted above waveforms indicate regions where the mixed model logistic regressions showed voltage to be significantly associated with errors (having $p_{FDR} < .01$ for more than 50 consecutive ms); light shaded bars correspond to congruent trials whereas dark bars correspond to incongruent trials. We looked for significant associations within the mean stimulus-response interval (SRI, labeled in the key). Mean dipoles for each of these clusters are plotted in the center on representative sagittal, axial, and coronal slices from the template brain. Abbreviations: dLFC = dorsolateral frontal cortex; MFC = medial frontal cortex; vLFC = ventrolateral frontal cortex; SMC = sensorimotor cortex; TC = temporal cortex; POC = parietooccipital cortex; OC = occipital cortex; the prefixes "a" and "p" refer to "anterior" and "posterior" (respectively) and suffixes "-L" and "-R" correspond to left and right hemispheres.

Error associations during the stimulus-response interval. Of the 15 putative brain source clusters, the only one for which we observed significant and consistent error associations across congruent and incongruent trials within the stimulus-response interval (i.e., the mean SRI between the dashed and solid vertical lines) was focused in pMFC (see navy blue arrows in upper

central of **Figure 4**). The mean scalp projection and subject dipoles for pMFC are plotted in **Figure 5**, which were primarily located in bilateral mid-cingulate cortex (39%) and supplementary motor area (21%) of the common template atlas (Tzourio-Mazoyer et al., 2002). In **Figure 6**, source contributions from this cluster (blue envelopes) to grand mean potentials across all channels (the mixture of all sources' and clusters' contributions, outer gray traces) are depicted, and accounted for approximately 5% to 14% of the variance of voltages reflected in scalp channels.

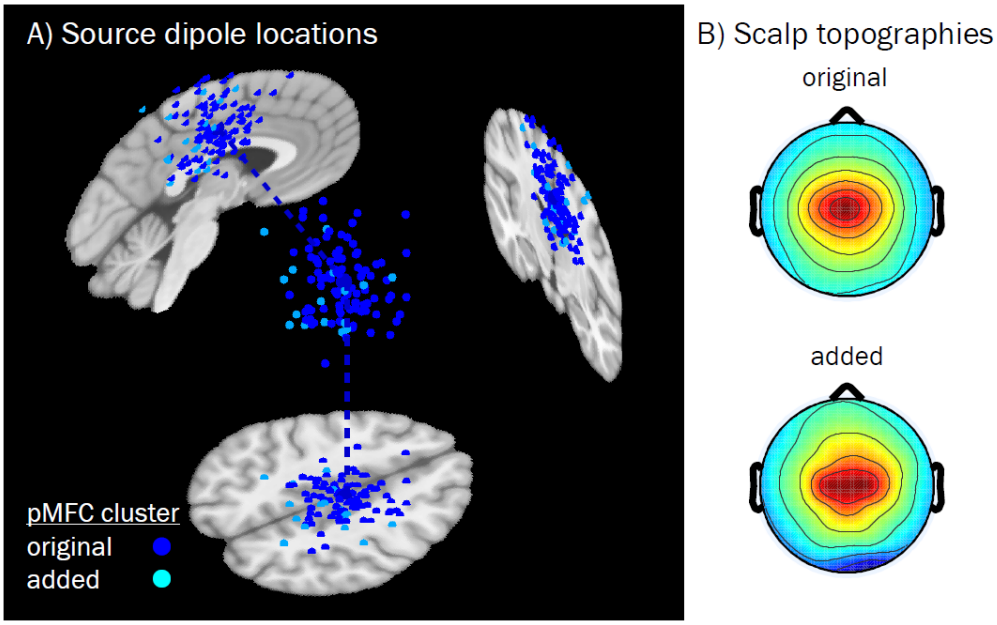

Figure 5. Equivalent current dipoles and mean scalp topographies for the pMFC source cluster derived by the k-means algorithm and *post hoc* additions. A) Subject dipoles and their projections onto MNI template space for pMFC are smaller in size than the cluster centroid (located in right mid-cingulate cortex, MNI coordinates: 4, -12, 44), which is larger. Blue subject dipoles depict sources that were included in the original k-means clustering output (n = 94, across 78 subjects); cyan dipoles correspond to sources that were added (for subjects with no dipole in the original cluster, n = 16) subsequently based on nearest distance in clustering measure space. B) Mean scalp topography for sources that were originally included in the k-means obtained pMFC cluster (above), and the topography for those sources which were subsequently added (below). Added subjects did not differ from the original pMFC-clustered subjects in terms of demographics (female vs. male: t[22] = -1.10, p = .284; age: t[21] = -.72, p = .477, Welch's two-sample t-test) or study variables of interest (error rate [log-transformed]: t[78] = 1.00, p = .319; ADHD symptoms [log-transformed]: t[78] = -1.48, p = .142, MLM linear regression). Note that while some dipole coordinates appear as being located outside of the brain for a given sagittal, coronal, or axial MRI slice (slices chosen based on the centroid coordinates), all dipoles were contained within the boundaries of the template brain as part of their inclusion criteria.

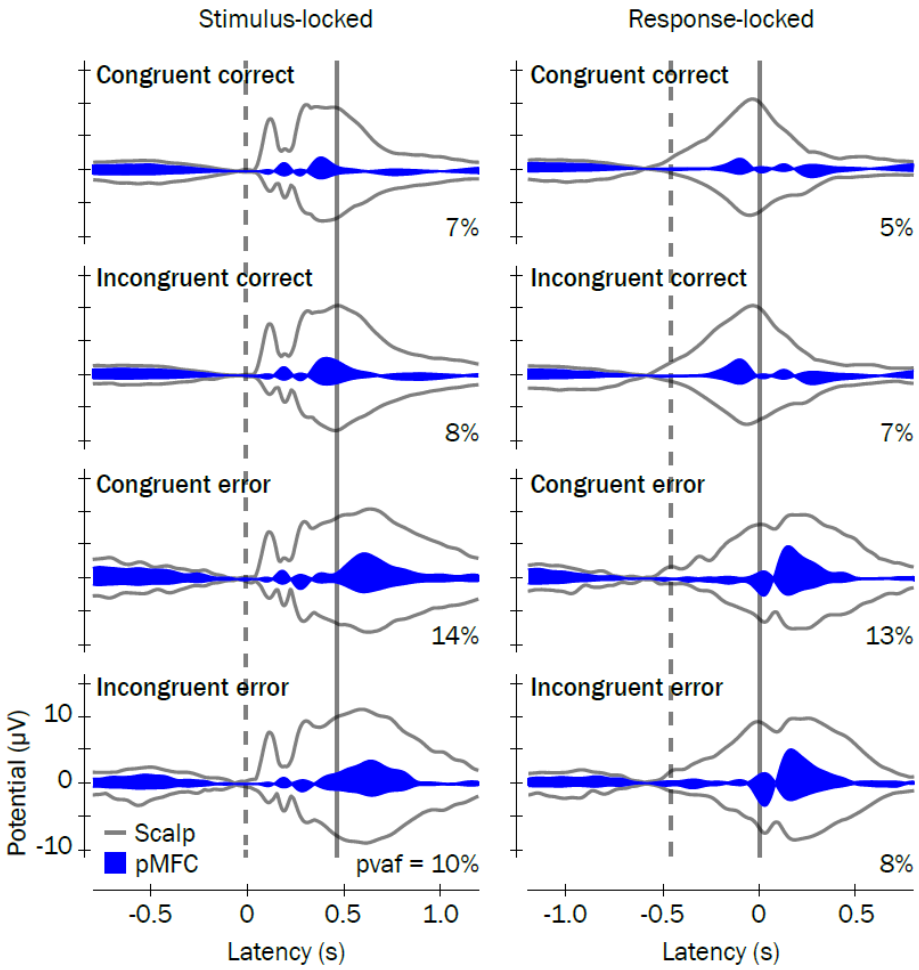

Figure 6. ERP envelopes and contributions of the pMFC cluster to scalp potentials. ERP envelopes (outer gray traces) show the maximum and minimum scalp channel voltages for each latency in the grand mean ERP waveforms, time-locked to stimulus presentations (left) and button responses (right). Grand mean latencies for stimulus presentations and button responses are denoted with vertical dashed and solid lines, respectively. Contributions of the pMFC source cluster to the grand mean ERPs are shown as blue envelopes and the percent variance accounted for ($pvaf_{sources} = 100 - 100 * \frac{mean(var(scalp\ data - scalp\ projection_{sources}))}{mean(var(scalp\ data))}$) by pMFC to each ERP envelope are reported.

We identified two vertex-projected positive-going peaks within pMFC-derived source waveforms for which the voltage within the SRI was more positive in correct performance trials than in error trials. These peaks occurred at approximately 390 ms after stimulus presentation in stimulus-locked waveforms and 110 ms before the response in response-locked waveforms and are labeled in **Figure 7A**. Because of the frontocentral midline scalp distribution of pMFC and the timings of these positive-going peaks relative to correct trial stimulus and response events, we termed these stimulus- and response-locked peaks as *Frontocentral P3* and *Pre-Movement Positivity (PMP)*, respectively.

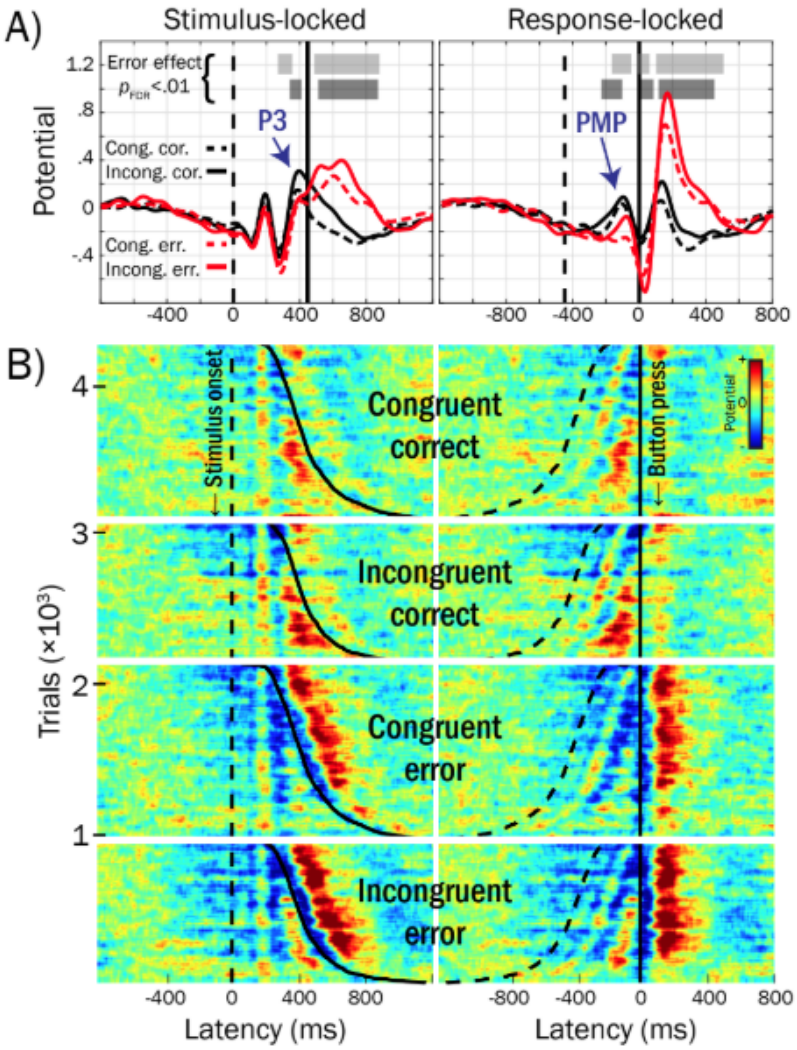

Figure 7. Grand mean waveforms from response-time-matched error and correct trials for the pMFC cluster activities and trial-level ERP-images. A) Voltage peaks within the mean stimulus-response interval (SRI, i.e., between the vertical dashed [stimulus] and solid [response] lines) that were associated with errors in trial-level logistic regressions are labeled: Frontocentral P3 and Pre-Movement Positivity (PMP). B) ERP-images for response-time-matched error and correct trials, across subjects. Stimulus- and response-locked ERP-images are labeled, reflecting time-varying voltage (referenced and scaled to baseline, see text) for each trial stacked and sorted by stimulus congruency (congruent, incongruent), response accuracy (error, correct), and response time (dashed line = stimulus onset, solid line = button press); red colors reflect positive voltage deflections and blues reflect negative voltage deflections (root mean square normalized within subject) forward-projected to channel Cz. Trials in ERP-images are grouped by congruent correct (*n* = 1,153), incongruent correct (*n* = 945), congruent error (*n* = 1,153) and incongruent error (*n* = 945). For example, the first row in the first group of trials corresponds to a correctly-performed congruent trial drawn from the subject with the fastest RT across all subjects; the last row in the first group of trials corresponds to a correctly-performed congruent trial from the subject with the slowest RT across all subjects. For ease of visualization, ERP images were smoothed vertically using a sliding boxcar window of 1% width the overall number of trials (*n* = 4,196).

Frontocentral P3 and PMP temporal relations to lateralized readiness potentials. We also examined error-related Frontocentral P3 and PMP temporal relations to lateralized readiness potentials (LRPs) thought to reflect central motor activation of the button press, enabling insight into whether error-related pMFC activations preceded brain activations reflecting the specific motor response to be carried out (i.e., left or right finger presses). In **Figure 8A**, grand mean waveforms averaged within correct (dashed traces) and error (solid traces) trials, separately for trials where the correct response required either left (green) or right (blue) button presses, are plotted for the pMFC cluster, as well as left (SMC-L) and right (SMC-R) clusters reflecting putative sensorimotor sources that were projected to scalp sites where LRPs are typically recorded. In **Figure 8B**, the polarity of LRPs (peaking approximately -75 ms in the response-locked ERP) encode the overt response hand mapping (contralateral hand / correct response = dashed trace; ipsilateral hand / error response = solid trace) and are labeled with navy arrows: in correct trials, the LRP is a negative-going voltage peak on the scalp contralateral to the finger press (reflecting activation of the correct motor response), whereas in error trials, the LRP is a positive-going peak on the scalp contralateral to the finger press (reflecting incorrect motor activation). PMP and LRP voltages were associated with errors at overlapping latencies, although PMP effects began earlier (-180 vs. -148 ms in response-locked waveforms), suggesting that error-related pMFC processes accompany and may begin before erroneous motor activations reflected in SMC.

Temporal overlap among stimulus- and response-locked processes. Stimulus presentation and button responses frequently occurred within close temporal proximity of one another, as visualized by dashed and solid traces (respectively) in the ERP-image plotted in **Figure 7B**. Here, each row (horizontal colored line) corresponds to pMFC source potential in a single trial plotted over time relative to stimulus (left) or response (right) events; red and blue hues indicate positive and negative voltage deflections, respectively. Frontocentral P3 and PMP peaks from **Figure 7A** appear in warm hues (reds, yellows) in **Figure 7B** that are consistent across rows at the same latencies. Importantly, temporal overlap resulting from tight succession of stimulus- and response-locked processes may result in confounding among Frontocentral P3 and PMP potentials.

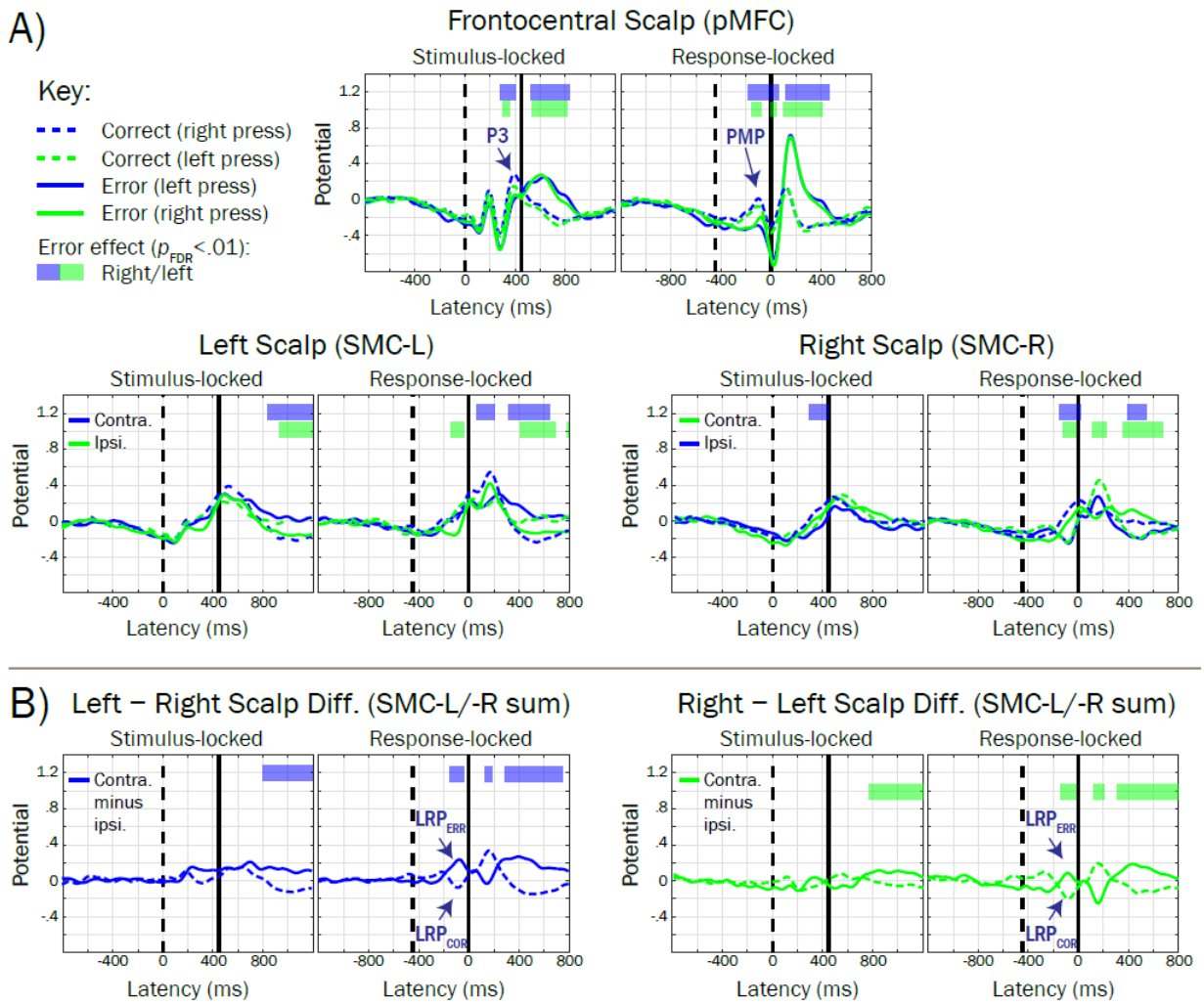

Figure 8. Grand mean trial waveforms reflecting posterior medial frontal cortex (pMFC) and lateralized motor-related potentials, and their association with errors. A) Grand mean waveforms for the pMFC source cluster and left (SMC-L, projected to site CP3) and right (SMC-R, CP4) clusters putatively reflecting sensorimotor cortical sources are averaged within trial accuracy (dashed trace = correct; solid trace = error) and the correct-response hand mapping (blue trace = right hand; green trace = left hand). Horizontal bars denote regions of the waveform that were significantly associated with errors (blue = correct-response right hand; green = correct-response left hand), accounting for a stimulus congruency interaction term. For comparability, trials and subjects contributing to SMC-L and SMC-R waveforms were identical to that of the pMFC cluster (unmatched subjects were included based on Euclidean distance in clustering measure space, see Method section). B) Lateralized readiness potentials (LRPs, labeled with navy arrows) were revealed by summing the scalp projections for SMC-L and SMC-R clusters, and subtracting the ipsilateral from contralateral waveform, consistent with guidelines reviewed by Smulders and Miller (2011). Note that the polarity of the LRP peak (approximately -75 ms in response-locked waveforms) in (B) encodes the response hand mapping, such that it is negative-going for correct contralateral responses (dashed trace; LRP_{COR}) and positive-going for erroneous ipsilateral responses (solid trace; LRP_{ERR}).

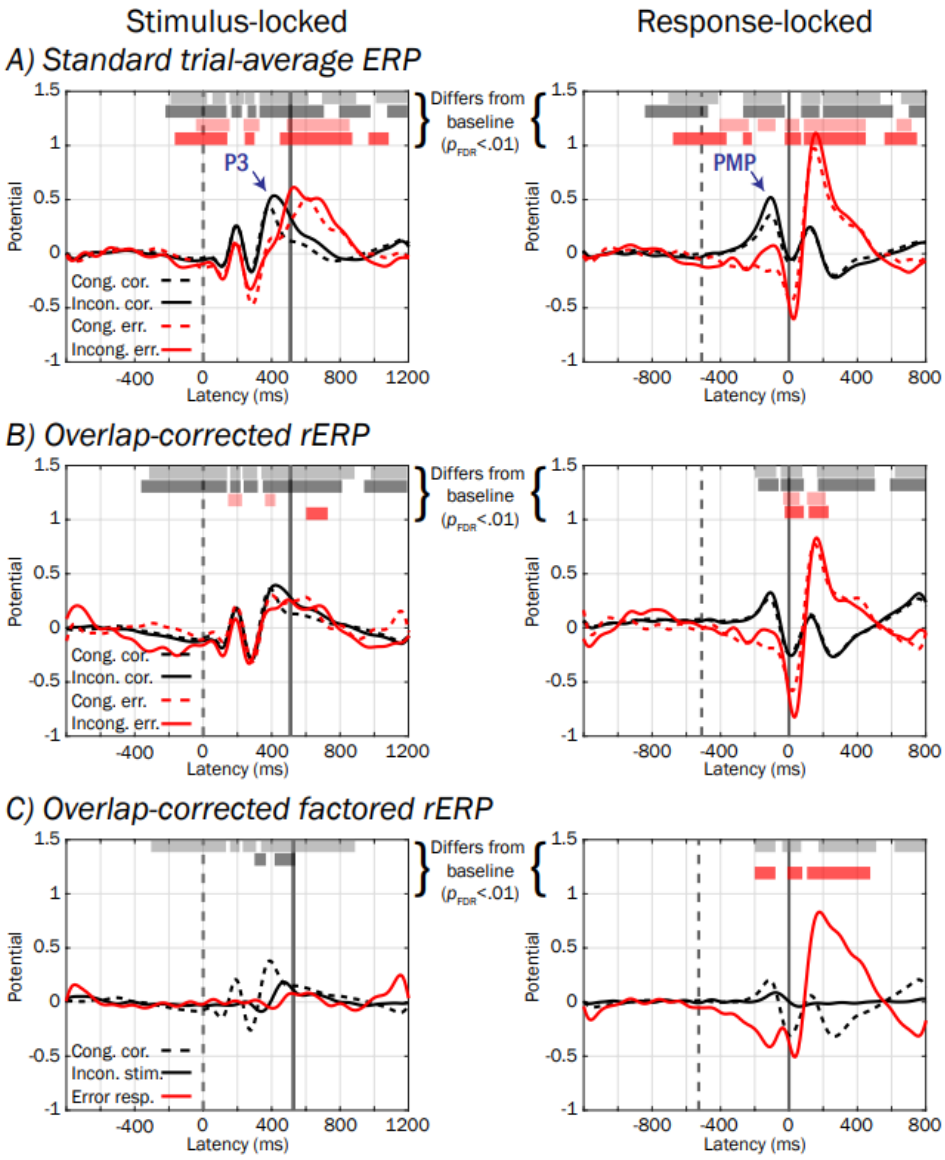

Figure 9. Standard ERPs, overlap-corrected rERPs, and overlap-corrected factored rERPs from the pMFC cluster. **A)** Standard trial-averaged stimulus- (left) and response-locked (right) ERPs, time-varying voltage of relatively consistent polarity at one or more latencies across trials (scaled to a pre-stimulus baseline period, see text) for each stimulus (congruent stimuli = dashed traces; incongruent = solid traces) and response type (correct = black; error = red). **B)** Overlap-corrected regression ERPs (rERPs, described in text) can be similarly interpreted to standard ERPs, although unlike standard ERPs that confound stimulus- and response-locked potentials occurring in the same time window, rERPs provide an estimate of what stimulus- and response-locked ERP processes separately contribute via summation to the time-overlapped standard ERP. **C)** Overlap-corrected, factored rERPs show the potential on congruent correct-performance trials (black dashed trace), 2) deviation when flanking stimuli are incongruent with the target stimulus (black solid trace), and 3) deviation associated with erroneous responses (red trace). The mean value within a pre-stimulus baseline interval was subtracted from all waveforms. Vertical dashed and solid lines denote mean stimulus and response latencies respectively.

Error associations within-subject using trial-aggregated ERP and rERPs. We next conducted analyses on standard trial-average ERPs and overlap-corrected rERPs, which estimate the evoked potential and suppress trial-to-trial variability in EEG traces. In **Figure 9**, waveforms are plotted showing (**A**) standard ERP trial averages and (**B**) overlap-corrected rERPs. Despite having comparable shapes, standard ERPs and overlap-corrected rERPs are not identical, as illustrated by horizontal bars reflecting latencies at which the amplitude of ERP/rERP waveforms deviated (p_{FDR} < .01) from the mean potential within the pre-stimulus baseline. Further, subtraction of rERP estimates from trial data adequately accounted for evoked potentials (see **Figure 10A-D**), whereas subtraction of standard ERPs from trial data does not and may introduce artifact (compare **Figure 10D-E**), suggesting superiority of the overlap-corrected rERP approach to standard ERPs for modeling single-trial evoked potentials. **Figure 9C** depicts the factored rERP waveforms for the expected ERP on congruent correct trials (black dashed trace), the event-related deviation when flanker stimuli are incongruent with the target stimulus (black solid trace), and the event-related deviation associated with erroneous responses (red trace). Factored rERPs highlight processes specific to stimulus type and response accuracy factors, which are confounded in **Figure 9A**-**B**.

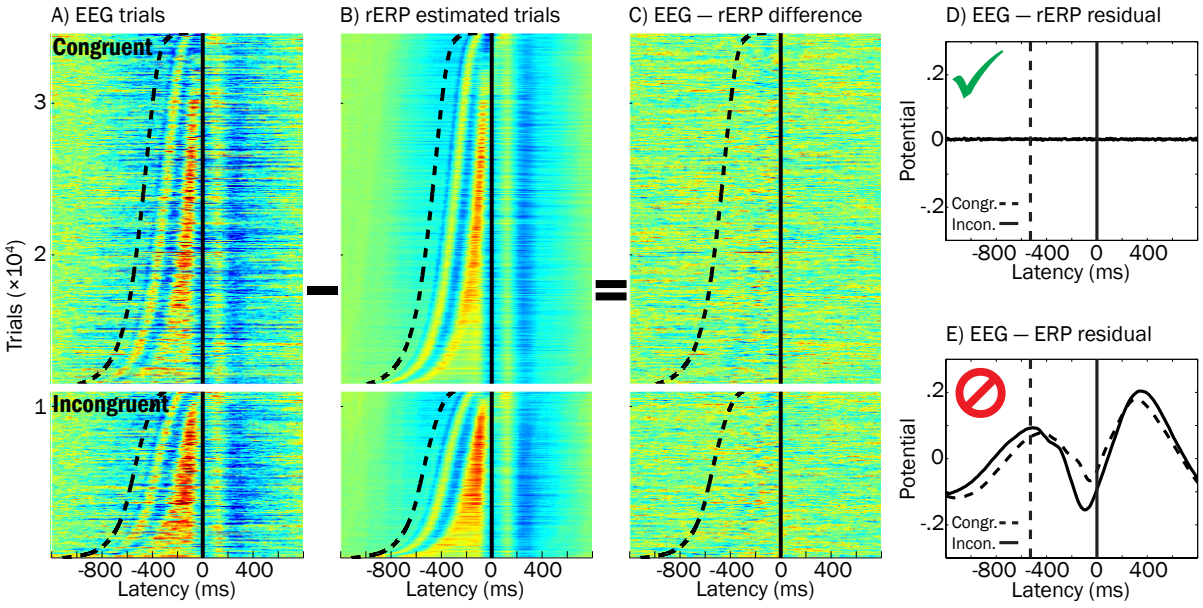

Figure 10. Effectiveness of using regression ERPs (rERPs) to account separately for stimulus and response processes that overlap in the single-trial EEG data. A) The "raw" response-locked ERP-image for all congruent and incongruent hit trials is plotted, sorted by response time. Sigmoidal dashed line and vertical solid line reflect stimulus and response latencies, respectively. B) Pseudo-data for rERP estimated trials was constructed by: 1) substituting each subject's response-locked rERP waveform (aligned to the button-press) in place of his or her trial data, and then 2) superimposing that subject's stimulus-locked rERP, shifted backwards in time with respect to stimulus onset. C) The ERP image from subtracting image (B)

from (A) is plotted to demonstrate that rERP is effective at removing stimulus and response potentials from trial EEG, as reflected by little consistencies in blue or red hues across trials. D) Grand average residual potentials after "EEG − rERP" (described above) and E) "EEG − ERP" (similar to above description, but substituting standard ERPs for overlap-corrected rERPs) illustrate superiority of the rERP approach to standard ERPs in modeling and accounting for trial evoked potentials. Note that the overlap-corrected rERP approach better accounts for overlapping stimulus and response potentials because the residual averaged ERP in (D) contains virtually no non-zero potentials while the same is not the case in (E).

Table 1

Association with errors using standard ERPs and overlap-corrected rERPs from the pMFC source cluster

			Standard trial-averaged ERP		
Trial type	Correct	Error		Logistic MLM	
ERP measure	*M* (*SD*)	*M* (*SD*)	B_{ERROR} (*SE*)	*OR* (95% CI)	*p*
Congruent					
Frontocentral P3	.33 (.42)	.08 (.64)	-.76 (.21)	.47 (.31, .70)	<.001*
PMP	.26 (.39)	-.18 (.42)	-1.60 (.30)	.21 (.11, .37)	<.001*
Incongruent					
Frontocentral P3	.44 (.50)	.05 (.60)	-1.19 (.30)	.30 (.17, .55)	<.001*
PMP	.41 (.48)	.03 (.51)	-1.10 (.28)	.35 (.20, .60)	<.001*
			Overlap-corrected regression-ERP (rERP)		
Trial type	Correct	Error		Logistic MLM	
rERP measure	*M* (*SD*)	*M* (*SD*)	B_{ERROR} (*SE*)	*OR* (95% CI)	*p*
Congruent					
Frontocentral P3	.28 (.33)	.18 (1.07)	-.17 (.19)	.84 (.59, 1.22)	.375
PMP	.13 (.31)	-.28 (1.03)	-.90 (.27)	.41 (.24, .69)	<.001*
Incongruent					
Frontocentral P3	.31 (.43)	.14 (.80)	-.42 (.23)	.66 (.42, 1.03)	.067
PMP	.17 (.36)	-.15 (.81)	-.86 (.31)	.42 (.23, .78)	.006*

Note. Descriptive statistics and results from logistic regressions predicting the log odds probability of an error response per one standard deviation positive change in voltages of standard ERP (top) or overlap-corrected regression ERP measures (rERP, bottom). Negative-valued B_{ERROR} and *OR*s smaller than 1 reflect greater odds of an error given lesser positivity (smaller amplitudes) of Frontocentral P3 (mean value within 340 to 440 ms in stimulus-locked waveforms) or PMP (-160 to -60 ms in response-locked waveforms). We used asterisks to highlight uncorrected *p*-values that survived correction for multiple comparisons at $p_{FDR} < .01$. Confidence intervals enable comparison of odds ratios at the $p < .05$ level. Other abbreviations: MLM = multi-level model; SE = standard error; PMP = Pre-Movement Positivity.

In **Table 1**, results from logistic regressions reflecting the influence of pMFC-derived Frontocentral P3 and PMP extracted from standard ERP (top) and overlap-corrected rERP (bottom) waveforms on probability of errors are presented. Consistent with the above trial-level analyses, more negative values for Frontocentral P3 and PMP derived from standard ERPs were associated with response errors ($p_{FDR} < .01$, top of **Table 1**). However, when derived from *overlap-corrected rERPs*, only PMP yielded significant associations with errors ($p_{FDR} < .01$) whereas Frontocentral P3 did not (range $p = .067$ to .375, bottom of **Table 1**). In addition, odds ratios for overlap-corrected Frontocentral P3 were significantly larger (closer to 1) than those for standard trial-averaged Frontocentral P3 in both congruent and incongruent trial types suggesting significantly weakened associations with errors, as evidenced by 95% confidence intervals for rERPs that did not contain odds ratios for ERPs. Thus, overlap-corrected rERP effects suggest that a smaller PMP (and not Frontocentral P3) is linked to errors (range *OR* = .41 to .42), and that overlap-correction substantially weakens the above error associations with Frontocentral P3.

Error associations within subjects using EEG-rERP trial residuals. Overlap-correction substantially diminished the strength of the association between smaller Frontocentral P3 and errors, suggesting that confounding from response-locked potentials (e.g., PMP) may have interjected error-related effects into stimulus-locked data. We tested this possibility by conducting logistic regressions on *EEG-rERP trial residuals*, which were calculated by subtracting stimulus- or response-locked rERPs from the "raw" trial-level source potentials. In **Figure 11**, trial residuals illustrate the associations of stimulus- and response-locked trial processes with errors, after removing overlapping stimulus-locked rERPs (**A**) or response-locked rERPs (**B**). Here, voltage negativity during the Frontocentral P3 and PMP time windows (dotted navy boxes) was significantly related to errors for both congruent and incongruent trials in the trial residuals for which stimulus-locked rERPs were subtracted (**A**), but not in the trial residuals for which response-locked rERPs were subtracted (**B**), confirming that response-locked rERP processes were predominantly driving error-related effects in both stimulus- and response-locked trial EEG potentials during the SRI.

By comparison with odds ratios obtained from logistic regressions conducted on the raw trial potentials (i.e., no subtraction of rERPs) within Frontocentral P3 (range *OR* = .80 to .88) and PMP (range *OR* = .76 to .82) time windows (see **Figure 11C**), associations obtained for trial residuals in which stimulus-locked rERPs were removed were stronger, as indicated odds ratios closer to 0 for Frontocentral P3 (range *OR* = .68 to .84) and PMP (range *OR* = .68 to .70). This reduction in odds ratio was significant for incongruent trials, such that the 95% confidence intervals for Frontocentral P3 and PMP did not contain odds ratios from the raw (no rERPs removed) trials. Collectively, results suggest that removal of stimulus-locked rERPs from trial potentials may clarify the association between smaller Frontocentral P3 / PMP trial potentials

and errors. By contrast, removal of response-locked rERPs resulted in opposite error associations (range *OR* = 1.09 to 1.22).

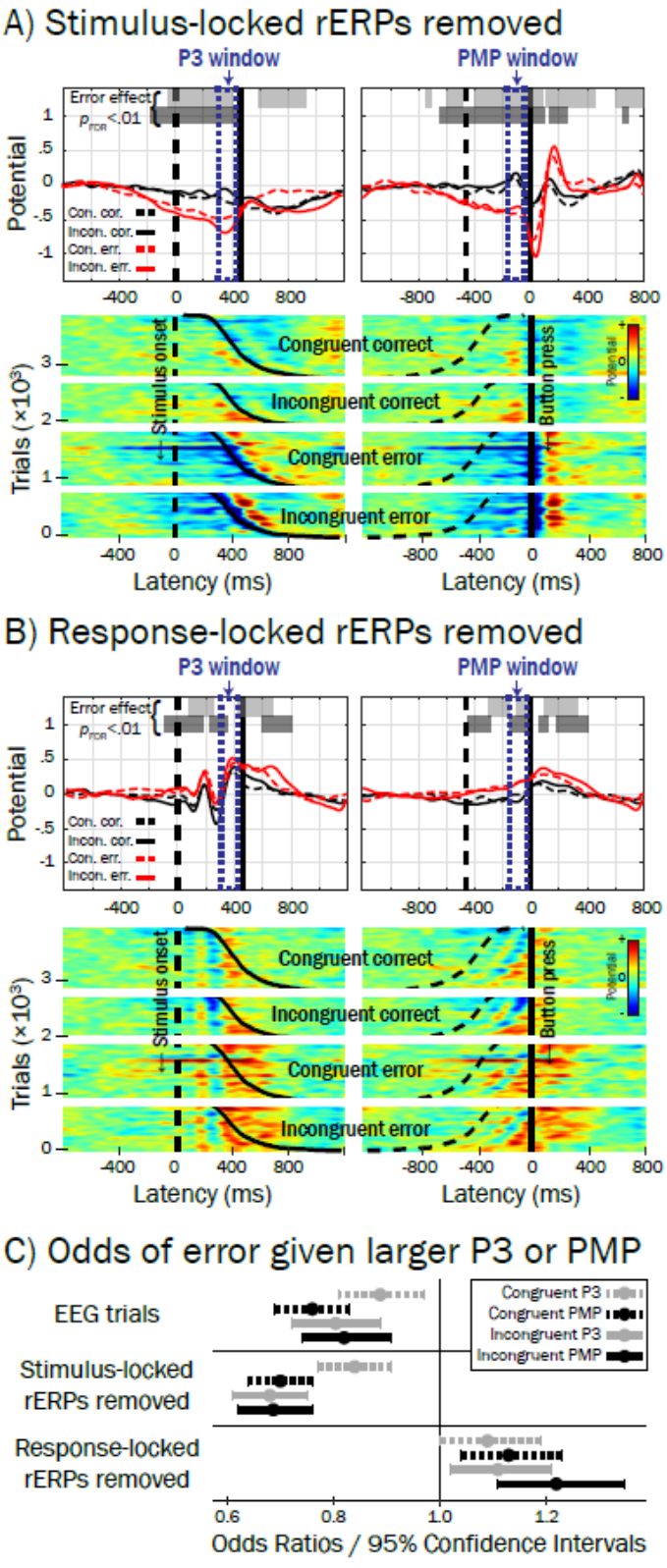

Figure 11. Error-related effects in pMFC trial residuals after subtraction of stimulus- or response-locked rERPs. A) Grand averages (upper) and ERP images (lower) reflecting stimulus- (left) and response-locked (right) trials that were constructed by subtracting the stimulus-locked rERP from "raw" trial potentials; 3,874 trials were drawn from only those participants who possessed at least six error trials and overlap-corrected rERPs (see Method section). Here, because stimulus-locked rERPs were removed from trial potentials, non-zero potentials in stimulus-locked residuals reflect confounding from response-locked processes. Horizontal bars plotted above waveforms indicate regions where logistic regression showed trial potentials were significantly related to the occurrence of an error (p_{FDR} < .01 for more than 50 consecutive ms) for congruent (light shaded bars) and incongruent trials (dark shaded bars); navy blue dotted boxes highlight Frontocentral P3 and Pre-Movement Positivity (PMP) windows in stimulus- and response-locked epochs, respectively. B) Trials constructed by subtracting response-locked rERPs from trial potentials; here, non-zero potentials in response-locked residuals reflect confounding from stimulus-locked processes. Notably, voltage negativity in Frontocentral P3 and PMP windows was associated with errors only in trial residuals for which stimulus-locked rERPs were removed (A). Vertical and sigmoidal-vertical lines in (A) and (B) reflect stimulus (dashed) and response (solid) latencies, respectively. C) Odds ratios (*OR*s, circles) less than 1 reflect greater odds of an error given more negativity in Frontocentral P3 / PMP windows in "raw" EEG trials (top, no rERPs subtracted). Removing stimulus-locked rERPs from trial EEG (middle)

strengthened associations between small Frontocentral P3 or PMP and errors, as indicated by comparatively smaller *OR*s and confidence intervals that do not contain *OR*s from raw EEG trials ($p < .05$, Incongruent P3 and PMP only). Removing response-locked rERPs (bottom) resulted in *OR*s that were greater than 1, suggesting that response-locked rERPs were responsible for prior associations between small single-trial Frontocentral P3 / PMP and errors.

Error-rate associations with stimulus congruency and ADHD symptom count. Overall, subjects possessed a mean error rate of 4.9% (*M* [*SD*] = 13.3 [12.6] trials) and 8.0% (*M* [*SD*] = 11.0 [10.5] trials) for congruent and incongruent stimuli (respectively), a statistically significant difference ($t[94] = 6.5$, $p < .001$, MLM linear regression). Additionally, ADHD symptom count across individuals was associated with elevated error rates on the task ($t[96] = 3.23$, $p = .002$, MLM linear regression), accounting for the main effect of stimulus congruency (incongruent vs. congruent, $t[137] = 4.50$, $p < .001$) and the interaction term (incongruent stimulus × ADHD symptoms, $t[137] = -.29$, $p = .774$).

Error rate associations between-subject using factored rERPs. Temporal windows in which pMFC source amplitude in the factored rERP waveforms were associated with between-subject differences ($p_{FDR} < .05$) in error rates are depicted by horizontal grey bars in **Figure 12**, as well as waveforms averaged within high (dashed trace) and low (solid trace) error rate tercile groups, reflecting relatively poor and good performers (respectively). Despite several latency regions being significantly associated with error rate (e.g., incongruent stimulus-locked P3, error response-locked negativity and positivity), only two of these latency regions in the response-locked waveforms temporally corresponded to the PMP window that we found above to correlate robustly with errors within the SRI, hereafter referred to as $PMP_{CORRECT}$ (-180 to -78 ms, PMP in reference level [i.e. congruent correct] trials in the rERP design, which contribute to all trial types) and $PMP_{INCONGRUENT}$ (-86 to -23 ms, positive deviation in PMP elicited by incongruent stimulus). Mean potentials extracted from these regions were used in remaining mediation analyses.

Do amplitude differences in rERPs mediate the association between ADHD symptom count and heightened task error rates? To test whether the main effect of ADHD symptom count on greater error rates might be mediated by "indirect effects" of the amplitudes of pMFC source potentials $PMP_{CORRECT}$ and $PMP_{INCONGRUENT}$ in the factored rERPs (see labeled regions marked with blue arrows in **Figure 12**), we computed paths in **Figure 3B** and presented the results in **Table 2**. Outcomes of mediation tests are shown in the rightmost column and denote whether the 95% confidence intervals for bootstrapped *ab* effects excluded zero, or equivalently, whether the reduction of the "total effect" of ADHD symptoms on error rate (path *c* in **Figure 3A**) to the "direct effect" (path *c'* in **Figure 3B**) was statistically significant.

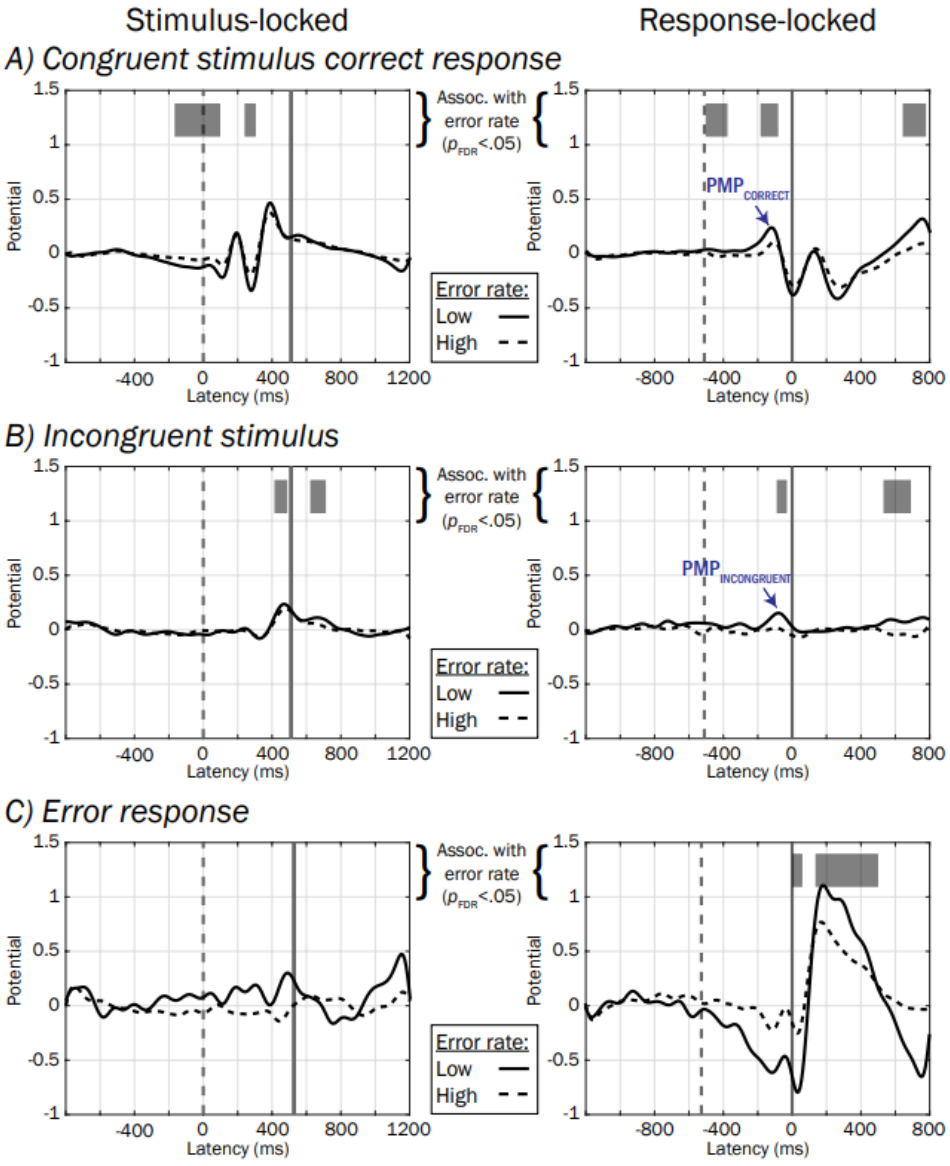

Figure 12. Between-subject voltage associations with error rates using factored rERPs. Waveforms depicting group averaged factored rERPs within high (dashed traces) and low (solid traces) error rates split by terciles are plotted for illustration. Periods of the factored rERPs are highlighted in greyscale to show regions where there was significant association (p_{FDR} < .05 for more than 50 contiguous ms) between rERP and error rate.

Table 2

Mediation of ADHD on task error rates using overlap-corrected, factored rERP amplitudes

	Indirect Effect		Direct Effect	Mediation
	a	*b*	*c'*	*ab*
	t (*df*)	*t* (*df*)	*t* (*df*)	*p*(|*ab*|)
$PMP_{CORRECT}$	-2.14 (62) *	-2.42 (82) *	2.35 (68) *	*
$PMP_{INCONGRUENT}$	-0.92 (59)	-1.96 (82)	2.96 (67) **	

Note. Results from mediation analyses, whereby the total effect of ADHD symptom count on overall task error rate has been partitioned into indirect (paths *a* and *b*) and direct (path *c'*) effects. Mediation has occurred when the reduction in total to direct effect is significant, or equivalently, when the magnitude of the indirect effect *ab* is significant ($p < .05$). T-statistics were computed by dividing linear regression coefficients by their standard errors; denominator degrees of freedom (*df*) were determined by Kenward-Roger approximation (see text). Significant paths are denoted by asterisks (* $p < .05$, ** $p < .01$).

Only one mediation test was significant, such that including the $PMP_{CORRECT}$ amplitude effect on error rates alongside ADHD symptoms resulted in a significant reduction of the total effect of ADHD on error rates. Collectively, the negatively-signed *a* path and significant mediation results suggest that reduced pMFC source amplitude in rERPs preceding correct responses during the SRI may partially explain the tendency for adolescents with more ADHD symptoms to make more errors on the task.

Discussion

We investigated brain potentials in the stimulus-response interval (SRI) during flanker task performance and examined voltage associations with errors, using EEG localized by ICA decomposition and equivalent dipole modeling of brain source processes in a sample of adolescents with varying degrees of ADHD symptoms. We found that smaller Frontocentral P3 and PMP peaks derived from pMFC, which typically occurred within the SRI, were associated with errors within subjects using trial-level and standard trial-averaged ERPs. Using a regression-ERP (rERP) technique to disambiguate overlapping stimulus- and response-locked brain potentials, the association with errors was attributed to smaller PMP and not Frontocentral P3, highlighting response-preceding pMFC processes (PMP) in discriminating correct from incorrect action selection. We also found smaller rERPs in the SRI to be associated with a larger subject error rate,

and that specifically a smaller $PMP_{CORRECT}$ mediated the strength of the association between ADHD symptom count and increased error rates.

Our observation of a positive shift in the electrical potential of pMFC sources within 200 ms before the button response in correct performance trials (PMP) is consistent with earlier research on movement-preceding ERPs (Deecke, Scheid, & Kornhuber, 1969; Delorme, Westerfield, & Makeig, 2007; Makeig et al., 1999; Roman, Brazdil, Jurak, Rektor, & Kukleta, 2005). The PMP may reflect a "go signal" (Bortoletto, Sarlo, Poli, & Stegagno, 2006; Deecke, Kornhuber, Lang, Lang, & Schreiber, 1985) by which supplementary motor areas (pre-SMA and SMA) stimulate a particular motor response to be carried out by circuits involving motor cortex. Indeed, PMP peaked earlier than LRPs projected from putative sensorimotor sources (-110 ms vs. -75 ms in response-locked ERPs) and we found significant reduction of PMP in pMFC sources on error trials approximately 30 ms before LRPs' indication of the incorrect motor activation. Thus, our data suggest that *a larger PMP precedes appropriate (vs. inappropriate) motor actions.* A similar effect has been observed for a subset of neurons in monkey pre-SMA which increase firing immediately before correct but not incorrect action selections (Isoda & Hikosaka, 2007). Pre-SMA is thought to facilitate "condition-action associations," such that conditions (e.g., tasks) require mapping of appropriate actions (here, button responses to target presentations) before action execution (Nachev, Kennard, & Husain, 2008). Perhaps the PMP generated by pMFC sources before correct responses reflects appropriate condition-action mapping in or near to pre-SMA, whereas on error trials this mapping is incomplete or inappropriate, reflected by a smaller PMP.

We also found smaller rERPs in waveform regions temporally overlapping with trial-level error effects ($PMP_{CORRECT}$, $PMP_{INCONGRUENT}$; see **Figure 12**) associated with higher subject error rate, and that a smaller $PMP_{CORRECT}$ mediated the association between subjects' ADHD symptom count and higher error rates. In our "treatment coding" rERP framework (Smith & Kutas, 2015a), $PMP_{CORRECT}$ was in the reference level factored rERP which contributes to response-locked potentials in all trial types (i.e., congruent correct reference trials, but also incongruent and erroneous response trials), suggesting that smaller PMP in poor performers and high ADHD symptomatic subjects is likely not specific to any particular trial type in this task.

To date, PMP has not been investigated with respect to ADHD, although other features of pre-response EEG (e.g., phase variability) have been shown to explain other facets of ADHD performance differences such as RT (e.g., McLoughlin et al., 2013). While it is not known whether the higher frequency of task errors exhibited by ADHD subjects is directly associated with "real-life" accident proneness (e.g., errors in motor vehicle operation; Vaa, 2014), our results suggest that PMP may have clinical implications. For instance, neuromodulation of MFC has improved cognitive performance in healthy individuals (e.g., Spieser, van den Wildenberg, Hasbroucq, Ridderinkhof, & Burle, 2015); perhaps similar "tuning" of pMFC using PMP as a target for

neuromodulation would prove useful in remediating accident proneness in patients with ADHD (e.g., Bloch et al., 2010).

It is important to emphasize that the PMP in our study should not be confused with the "error-preceding positivity" described by other researchers (Allain et al., 2004; Hajcak et al., 2005; Ridderinkhof et al., 2003), which refers to a reduction in the correct-response negativity (Ford, 1999) in the *trial* before the error trial and does not enable insight into action selection brain dynamics within the SRI on the error trial itself (as does PMP). Instead, we believe a related frontocentral scalp-recorded brain potential to the PMP to be the peak preceding the error-related negativity (ERN) noted by others (e.g., Albrecht et al., 2010; Albrecht et al., 2008; Cavanagh, Cohen, & Allen, 2009; Debener et al., 2005; Falkenstein, Hoormann, & Hohnsbein, 2001; McLoughlin et al., 2009; Nieuwenhuis, Ridderinkhof, Blom, Band, & Kok, 2001), which has been used (subtracted) for the purpose of quantifying ERN effects but otherwise overlooked. We speculate that PMP might also be conflated with other stimulus-locked ERP peaks that typically precede speeded manual responses such as frontally-focused P2 and P3 waves (e.g., Delorme et al., 2007; Makeig, Delorme, et al., 2004; Makeig et al., 1999; Perri et al., 2015; Potts, Liotti, Tucker, & Posner, 1996; Wessel & Aron, 2015). Indeed, in **Table 1** we found the amplitude of Frontocentral P3 to be strongly associated with errors in standard ERPs ($p < .001$), but that these associations were essentially absent after correcting for overlap with response-locked potentials ($p > .067$), suggesting that temporal confounding is perhaps responsible for Frontocentral P3's seeming association with errors.

Limitations. It is important to note that because we neither manipulated the size of brain potentials, nor manipulated other factors (e.g., ADHD) influencing task performance, we cannot infer that the size of PMP (or another factor) plays a causal role in determining task accuracy for a given trial or individual. In future research, we speculate that applying neuromodulation (e.g., noninvasive brain stimulation) to pMFC to modulate PMP amplitude, it may be possible to evaluate such a causal hypothesis.

Consistent with previous ERP studies using flanker tasks (see review by Folstein & Van Petten, 2008), responses were recorded with button presses rather than electromyograms (EMGs), precluding investigation of dynamics accompanying central motor conductance timing (CMCTs, delays between motor brain potentials and EMG responses) and EMG onset-to-button press timing (e.g., "partial errors"; Roger et al., 2014). While we cannot know how CMCT- and EMG-induced dynamics might influence the latencies of brain potentials in our study, we conjecture that such effects are small (e.g., CMCTs typically range 3 to 5 milliseconds in humans aged > 4 years; Udupa & Chen, 2013) or relatively constant (i.e., shifting waveforms' latencies by some fixed delay) given the tight succession of EMG and button presses. Crucially, we observed PMP concurrently with well-known ERP features, such as LRPs, that typically precede EMG

responses. To the extent that PMP effects accompany or precede LRPs (or other lateralized motor signals; e.g., Fischer, Nigbur, Klein, Danielmeier, & Ullsperger, 2018; Pape & Siegel, 2016), it may be supposed that they also tend to accompany or precede EMG onsets.

Trial-level analyses and overlap-corrected rERP approaches used here are not without their limitations. First, one might question the comparability of RT-matched error and correct trials, given that on average, RTs for error trials were typically shorter than those for correct trials. Although RT was included as a covariate in trial-level logistic regressions to account for main effects of RT on the probability of an error, an effective way that future research might investigate the comparability of waveforms belonging to short-, medium-, and long-RT trials might be to study "typical RT" error and correct trials in three versions of the task having short-, medium-, and long-response windows (respectively), instead of the fixed response window we used here.

Relatedly, due to a limited number of trials with limited range in RTs (e.g., standard deviations for the four trial types ranged about 144 to 192 ms, see Method section), it is possible that some of the hypothetical overlap in stimulus- and response-locked processes contained in overlap-corrected rERPs may not be adequately dissociated, such that there may be residual "smearing" in stimulus- and response-locked rERPs (see discussions on RT and interstimulus-interval effects in Smith and Kutas, 2015a,b). Future research with more trials and larger range in RTs may be useful to better model overlap and RT effects.

The spread of brain locations of the equivalent dipoles in the pMFC source cluster appears larger than expected with a single functional brain region (see Tsai, Jung, Chien, Savostyanov, & Makeig, 2014). Dipole localization errors may have added to this spread; these could arise from insufficiencies in subject head models (e.g., inaccurate skull conductivity; Akalin Acar & Makeig, 2013), or in poor co-registration of scalp electrode positions, and hence the subject dipoles, to the MNI template head. Skull conductivity varies across individuals due to several factors (e.g., development) but was held constant here across subjects, as a noninvasive method for its estimation within-subject (Akalin Acar, Acar, & Makeig, 2016) was not yet readily available. Lastly, pMFC source clusters originally obtained by the k-means algorithm did not include all subjects, necessitating *post hoc* addition of outlier sources from k-means non-included subjects for the sake of preserving sample size and statistical power. Although this step may introduce possible inhomogeneities in the clusters themselves, added sources appeared comparable to original sources (e.g., **Figure 5**).

Conclusions. Using source-localized EEGs resolved by ICA decomposition and subject-specific head models, we found that smaller PMP amplitudes projected from pMFC, typically occurring within the SRI, were robustly associated with flanker task error commission in trial-level EEG,

trial-averaged ERPs, and overlap-corrected rERPs. Smaller stimulus-locked Frontocentral P3 was associated with errors in trial-level and trial-averaged ERPs, but not in overlap-corrected rERPs, collectively underlining the importance of motor (PMP) versus perceptual (Frontocentral P3) processes in trial performance. Finally, having more ADHD symptoms was associated with producing higher error rates and smaller PMP partially mediated this association.

Notably, the ICA source decomposition, dipole modeling, and rERP methodologies used in the present article aided in discovery and characterization of novel error-related effects during the SRI. Potential advantages of ICA and dipole localization for disentangling effective brain signals of interest from other brain and nonbrain sources have been detailed elsewhere (Loo, Lenartowicz, & Makeig, 2016; Makeig, Debener, Onton, & Delorme, 2004; Makeig et al., 2012; McLoughlin, Makeig, & Tsuang, 2014; Mullen et al., 2015). Here, because the EEG effective source cluster near pMFC where we found PMP effects of interest contributed relatively little to scalp potentials (5% to 14%; **Figure 6**), PMP's association with errors may be otherwise masked or confounded in scalp EEGs.

To the extent that temporally proximal events (e.g., stimulus presentations and button responses in fast-paced tasks) lead to temporal confounding of overlapping processes in standard ERPs and trial-level EEG, rERP methods may be used to correct for such overlap (e.g., **Figure 9**) and/or remove such overlapping processes from trial data (e.g., generate trial residuals, **Figure 11**). While the rERP models used here were chosen because they reflect a straightforward overlap-corrected extension of standard ERPs, the flexible nature of the rERP technique (Ehinger & Dimigen, 2018; Smith & Kutas, 2015a, 2015b) enables modeling of other (e.g., nonlinear) effects that may be involved in erroneous task performance and ADHD.

We propose that reduced PMP could be a valuable target for intervention as well as being possibly useful as a developmental endophenotypic biomarker reflecting genetic risk for error proneness in psychopathology including ADHD (cf. Burwell et al., 2016; Iacono & Malone, 2011; Iacono, Malone, & Vrieze, 2016). Indeed, PMP amplitudes in response-locked rERPs from correct trials were similar among the identical twin pairs who participated in the present investigation (intra-class correlation = .29, p = .023), reflecting familial influences. The putative genetic basis of PMP remains to be investigated, but it is possible that the source decomposition and/or rERP methodologies used in our study could aide in clarifying the degree to which brain potentials reliably tap into vulnerability mechanisms underlying psychopathology, which may have been otherwise masked or confounded in scalp EEG recordings and standard ERPs (Loo et al., 2016; McLoughlin et al., 2014). Additionally, the mutability of PMP remains to be delineated, but prior neuromodulation of pMFC has yielded increased cerebral blood flow in pre-SMA (Obeso et al., 2013) and enhanced inhibitory network connectivity (Watanabe et al., 2015), suggesting that similar efforts to modulate PMP may be productive. Regardless, our results bolster the

importance of response-preceding ERPs projected from pMFC during the SRI in discriminating correct and erroneous action selections. In future research, PMP may be useful in predictive modeling of error commissions during task performance (e.g., Bode & Stahl, 2014; Yamane, Nambu, & Wada, 2014) and predicting error proneness in ADHD.

Acknowledgements: This research was made possible by funding from grant number AA017314 from the National Institute of Alcohol Abuse and Alcoholism (NIAAA) as well as grant numbers DA036216 and DA05147 from the National Institute on Drug Abuse (NIDA). In addition, SJB is funded by a NIDA T32 postdoctoral fellowship (DA037183) and received funding from the Society for Psychophysiological Research that enabled mentorship from SM at the Swartz Center for Computational Neuroscience (SCCN) at UCSD. SJB would like to acknowledge Shelby Piepho for assistance with manual preprocessing of structural MRI images as part of an undergraduate research experience. Also, SJB would like to thank Dr. Zeynep Akalin Acar and Matthew Burns at the SCCN for providing feedback in computational head modeling and regression ERP procedures (respectively), as well as Dr. Philip Burton at UMN's Center for Magnetic Resonance Research for his expert guidance in the cross-subject dipole co-registration method. SM's participation was funded by a gift from The Swartz Foundation (Old Field, NY).

Keywords: ERP, stimulus-response interval, pre-movement positivity, performance monitoring, ADHD, medial frontal cortex

References

Acar, Z. A., & Makeig, S. (2010). Neuroelectromagnetic forward head modeling toolbox. *J Neurosci Methods, 190*(2), 258-270. doi: 10.1016/j.jneumeth.2010.04.031

Agresti, A. (2013). *Categorical data analysis* (3rd ed.). Hoboken, NJ: Wiley.

Akalin Acar, Z., Acar, C. E., & Makeig, S. (2016). Simultaneous head tissue conductivity and EEG source location estimation. *Neuroimage, 124*(Pt A), 168-180. doi: 10.1016/j.neuroimage.2015.08.032

Akalin Acar, Z., & Makeig, S. (2013). Effects of forward model errors on EEG source localization. *Brain Topogr, 26*(3), 378-396. doi: 10.1007/s10548-012-0274-6

Albrecht, B., Brandeis, D., Uebel, H., Heinrich, H., Heise, A., Hasselhorn, M., . . . Banaschewski, T. (2010). Action monitoring in children with or without a family history of ADHD--effects of gender on an endophenotype parameter. *Neuropsychologia, 48*(4), 1171-1177. doi: 10.1016/j.neuropsychologia.2009.12.018

Albrecht, B., Brandeis, D., Uebel, H., Heinrich, H., Mueller, U. C., Hasselhorn, M., . . . Banaschewski, T. (2008). Action monitoring in boys with attention-deficit/hyperactivity disorder, their nonaffected siblings, and normal control subjects: evidence for an endophenotype. *Biol Psychiatry, 64*(7), 615-625. doi: 10.1016/j.biopsych.2007.12.016

Allain, S., Carbonnell, L., Falkenstein, M., Burle, B., & Vidal, F. (2004). The modulation of the Ne-like wave on correct responses foreshadows errors. *Neurosci Lett, 372*(1-2), 161-166. doi: 10.1016/j.neulet.2004.09.036

American Psychiatric Association. (2000). Diagnostic and statistical manual of mental disorders: DSM-IV-TR. Washington, DC: American Psychiatric Association.

Anokhin, A. P., & Golosheykin, S. (2015). Neural correlates of error monitoring in adolescents prospectively predict initiation of tobacco use. *Dev Cogn Neurosci, 16*, 166-173. doi: 10.1016/j.dcn.2015.08.001

Bach, D. R., Flandin, G., Friston, K. J., & Dolan, R. J. (2010). Modelling event-related skin conductance responses. *Int J Psychophysiol, 75*(3), 349-356. doi: 10.1016/j.ijpsycho.2010.01.005

Baumann, S. B., Wozny, D. R., Kelly, S. K., & Meno, F. M. (1997). The electrical conductivity of human cerebrospinal fluid at body temperature. *IEEE Trans Biomed Eng, 44*(3), 220-223. doi: 10.1109/10.554770

Behmer, L. P., Jr., & Fournier, L. R. (2016). Mirror neuron activation as a function of explicit learning: changes in mu-event-related power after learning novel responses to ideomotor compatible, partially compatible, and non-compatible stimuli. *Eur J Neurosci, 44*(10), 2774-2785. doi: 10.1111/ejn.13389

Benjamini, Y., & Hochberg, Y. (1995). Controlling the False Discovery Rate - a Practical and Powerful Approach to Multiple Testing. *Journal of the Royal Statistical Society Series B-Methodological, 57*(1), 289-300.

Bloch, Y., Harel, E. V., Aviram, S., Govezensky, J., Ratzoni, G., & Levkovitz, Y. (2010). Positive effects of repetitive transcranial magnetic stimulation on attention in ADHD Subjects: a randomized controlled pilot study. *World J Biol Psychiatry, 11*(5), 755-758. doi: 10.3109/15622975.2010.484466

Bode, S., & Stahl, J. (2014). Predicting errors from patterns of event-related potentials preceding an overt response. *Biol Psychol, 103*, 357-369. doi: 10.1016/j.biopsycho.2014.10.002

Bortoletto, M., Sarlo, M., Poli, S., & Stegagno, L. (2006). Pre-motion positivity during self-paced movements of finger and mouth. *Neuroreport, 17*(9), 883-886. doi: 10.1097/01.wnr.0000221830.95598.ea

Brook, U., & Boaz, M. (2006). Adolescents with attention deficit and hyperactivity disorder/learning disability and their proneness to accidents. *Indian J Pediatr, 73*(4), 299-303.

Burns, M. D., Bigdely-Shamlo, N., Smith, N. J., Kreutz-Delgado, K., & Makeig, S. (2013). Comparison of averaging and regression techniques for estimating Event Related Potentials. *Conf Proc IEEE Eng Med Biol Soc, 2013*, 1680-1683. doi: 10.1109/EMBC.2013.6609841

Burwell, S. J., Malone, S. M., Bernat, E. M., & Iacono, W. G. (2014). Does electroencephalogram phase variability account for reduced P3 brain potential in externalizing disorders? *Clin Neurophysiol, 125*(10), 2007-2015. doi: 10.1016/j.clinph.2014.02.020

Burwell, S. J., Malone, S. M., & Iacono, W. G. (2016). One-year developmental stability and covariance among oddball, novelty, go/no-go, and flanker event-related potentials in adolescence: A monozygotic twin study. *Psychophysiology, 53*(7), 991–1007. doi: 10.1111/psyp.12646

Cavanagh, J. F., Cohen, M. X., & Allen, J. J. (2009). Prelude to and resolution of an error: EEG phase synchrony reveals cognitive control dynamics during action monitoring. *J Neurosci, 29*(1), 98-105. doi: 10.1523/JNEUROSCI.4137-08.2009

Cohen, M. X., & Cavanagh, J. F. (2011). Single-trial regression elucidates the role of prefrontal theta oscillations in response conflict. *Front Psychol, 2*, 30. doi: 10.3389/fpsyg.2011.00030

Cox, R. W. (1996). AFNI: software for analysis and visualization of functional magnetic resonance neuroimages. *Comput Biomed Res, 29*(3), 162-173.

de Jong, R., Wierda, M., Mulder, G., & Mulder, L. J. (1988). Use of partial stimulus information in response processing. *J Exp Psychol Hum Percept Perform, 14*(4), 682-692.

Debener, S., Thorne, J., Schneider, T. R., & Viola, F. C. (2010). Using ICA for the analysis of multi-channel EEG data. In M. Ullsperger & S. Debener (Eds.), *Simultaneous EEG and fMRI: Recording, Analysis, and Application 1st Edition*.

Debener, S., Ullsperger, M., Siegel, M., Fiehler, K., von Cramon, D. Y., & Engel, A. K. (2005). Trial-by-trial coupling of concurrent electroencephalogram and functional magnetic

resonance imaging identifies the dynamics of performance monitoring. *J Neurosci, 25*(50), 11730-11737. doi: 10.1523/JNEUROSCI.3286-05.2005

Deecke, L., Kornhuber, H. H., Lang, W., Lang, M., & Schreiber, H. (1985). Timing function of the frontal cortex in sequential motor and learning tasks. *Hum Neurobiol, 4*(3), 143-154.

Deecke, L., Scheid, P., & Kornhuber, H. H. (1969). Distribution of Readiness Potential, Pre-motion Positivity, and Motor Potential of the Human Cerebral Cortex Preceding Voluntary Finger Movements. *Exp Brain Res, 7*(2), 158-168.

Delorme, A., & Makeig, S. (2004). EEGLAB: an open source toolbox for analysis of single-trial EEG dynamics including independent component analysis. *J Neurosci Methods, 134*(1), 9-21. doi: 10.1016/j.jneumeth.2003.10.009

Delorme, A., Palmer, J., Onton, J., Oostenveld, R., & Makeig, S. (2012). Independent EEG sources are dipolar. *PLoS One, 7*(2), e30135. doi: 10.1371/journal.pone.0030135

Delorme, A., Westerfield, M., & Makeig, S. (2007). Medial prefrontal theta bursts precede rapid motor responses during visual selective attention. *J Neurosci, 27*(44), 11949-11959. doi: 10.1523/JNEUROSCI.3477-07.2007

Ehinger, B. V., & Dimigen, O. (2018). Unfold: An integrated toolbox for overlap correction, non-linear modeling, and regression-based EEG analysis. *bioRxiv*. doi: 10.1101/360156

Ehinger, B. V., Fischer, P., Gert, A. L., Kaufhold, L., Weber, F., Pipa, G., & Konig, P. (2014). Kinesthetic and vestibular information modulate alpha activity during spatial navigation: a mobile EEG study. *Front Hum Neurosci, 8*, 71. doi: 10.3389/fnhum.2014.00071

Eichele, T., Debener, S., Calhoun, V. D., Specht, K., Engel, A. K., Hugdahl, K., . . . Ullsperger, M. (2008). Prediction of human errors by maladaptive changes in event-related brain networks. *Proc Natl Acad Sci U S A, 105*(16), 6173-6178. doi: 10.1073/pnas.0708965105

Eriksen, B. A., & Eriksen, C. W. (1974). Effects of Noise Letters Upon Identification of a Target Letter in a Nonsearch Task. *Percept Psychophys, 16*(1), 143-149. doi: Doi 10.3758/Bf03203267

Falkenstein, M., Hoormann, J., & Hohnsbein, J. (2001). Changes of error-related ERPs with age. *Exp Brain Res, 138*(2), 258-262.

Fischer, A. G., Nigbur, R., Klein, T. A., Danielmeier, C., & Ullsperger, M. (2018). Cortical beta power reflects decision dynamics and uncovers multiple facets of post-error adaptation. *Nat Commun, 9*(1), 5038. doi: 10.1038/s41467-018-07456-8

Folstein, J. R., & Van Petten, C. (2008). Influence of cognitive control and mismatch on the N2 component of the ERP: a review. *Psychophysiology, 45*(1), 152-170. doi: 10.1111/j.1469-8986.2007.00602.x

Ford, J. M. (1999). Schizophrenia: the broken P300 and beyond. *Psychophysiology, 36*(6), 667-682.

Geddes, L. A., & Baker, L. E. (1967). The specific resistance of biological material--a compendium of data for the biomedical engineer and physiologist. *Med Biol Eng, 5*(3), 271-293.

Gramann, K., Onton, J., Riccobon, D., Mueller, H. J., Bardins, S., & Makeig, S. (2010). Human brain dynamics accompanying use of egocentric and allocentric reference frames during navigation. *J Cogn Neurosci, 22*(12), 2836-2849. doi: 10.1162/jocn.2009.21369

Gratton, G., Coles, M. G., Sirevaag, E. J., Eriksen, C. W., & Donchin, E. (1988). Pre- and poststimulus activation of response channels: a psychophysiological analysis. *J Exp Psychol Hum Percept Perform, 14*(3), 331-344.

Hajcak, G., Nieuwenhuis, S., Ridderinkhof, K. R., & Simons, R. F. (2005). Error-preceding brain activity: robustness, temporal dynamics, and boundary conditions. *Biol Psychol, 70*(2), 67-78. doi: 10.1016/j.biopsycho.2004.12.001

Hinrichs, H., Scholz, M., Tempelmann, C., Woldorff, M. G., Dale, A. M., & Heinze, H. J. (2000). Deconvolution of event-related fMRI responses in fast-rate experimental designs: tracking amplitude variations. *J Cogn Neurosci, 12 Suppl 2*, 76-89. doi: 10.1162/089892900564082

Iacono, W. G., & Malone, S. M. (2011). Developmental Endophenotypes: Indexing Genetic Risk for Substance Abuse with the P300 Brain Event-Related Potential. *Child Dev Perspect, 5*(4), 239-247. doi: 10.1111/j.1750-8606.2011.00205.x

Iacono, W. G., Malone, S. M., & Vrieze, S. I. (2016). Endophenotype best practices. *Int J Psychophysiol*. doi: 10.1016/j.ijpsycho.2016.07.516

Isoda, M., & Hikosaka, O. (2007). Switching from automatic to controlled action by monkey medial frontal cortex. *Nat Neurosci, 10*(2), 240-248. doi: 10.1038/nn1830

Jerome, L., Habinski, L., & Segal, A. (2006). Attention-deficit/hyperactivity disorder (ADHD) and driving risk: a review of the literature and a methodological critique. *Curr Psychiatry Rep, 8*(5), 416-426.

Knaepen, K., Mierau, A., Swinnen, E., Fernandez Tellez, H., Michielsen, M., Kerckhofs, E., . . . Meeusen, R. (2015). Human-Robot Interaction: Does Robotic Guidance Force Affect Gait-Related Brain Dynamics during Robot-Assisted Treadmill Walking? *PLoS One, 10*(10), e0140626. doi: 10.1371/journal.pone.0140626

Kosten, T. A., & Rounsaville, B. J. (1992). Sensitivity of psychiatric diagnosis based on the best estimate procedure. *Am J Psychiatry, 149*(9), 1225-1227. doi: 10.1176/ajp.149.9.1225

Kuznetsova, A., Brockhoff, P. B., & Bojesen Christensen, R. H. (2016). Tests in Linear Mixed Effects Models.

Lai, Y., van Drongelen, W., Ding, L., Hecox, K. E., Towle, V. L., Frim, D. M., & He, B. (2005). Estimation of in vivo human brain-to-skull conductivity ratio from simultaneous extra- and intra-cranial electrical potential recordings. *Clin Neurophysiol, 116*(2), 456-465. doi: 10.1016/j.clinph.2004.08.017

Leckman, J. F., Sholomskas, D., Thompson, W. D., Belanger, A., & Weissman, M. M. (1982). Best estimate of lifetime psychiatric diagnosis: a methodological study. *Arch Gen Psychiatry, 39*(8), 879-883.

Lijffijt, M., Kenemans, J. L., Verbaten, M. N., & van Engeland, H. (2005). A meta-analytic review of stopping performance in attention-deficit/hyperactivity disorder: deficient inhibitory motor control? *J Abnorm Psychol, 114*(2), 216-222. doi: 10.1037/0021-843X.114.2.216

Lisi, G., & Morimoto, J. (2015). EEG Single-Trial Detection of Gait Speed Changes during Treadmill Walk. *PLoS One, 10*(5), e0125479. doi: 10.1371/journal.pone.0125479

Loo, S. K., Lenartowicz, A., & Makeig, S. (2016). Research Review: Use of EEG biomarkers in child psychiatry research - current state and future directions. *J Child Psychol Psychiatry, 57*(1), 4-17. doi: 10.1111/jcpp.12435

Luck, S. J. (2005). Ten Simple Rules for Designing and Interpreting ERP Experiments. In T. C. Handy (Ed.), *Event-Related Potentials: A Methods Handbook*: MIT Press.

Luu, P., Tucker, D. M., & Makeig, S. (2004). Frontal midline theta and the error-related negativity: neurophysiological mechanisms of action regulation. *Clin Neurophysiol, 115*(8), 1821-1835. doi: 10.1016/j.clinph.2004.03.031

Makeig, S., Debener, S., Onton, J., & Delorme, A. (2004). Mining event-related brain dynamics. *Trends Cogn Sci, 8*(5), 204-210. doi: 10.1016/j.tics.2004.03.008

Makeig, S., Delorme, A., Westerfield, M., Jung, T. P., Townsend, J., Courchesne, E., & Sejnowski, T. J. (2004). Electroencephalographic brain dynamics following manually responded visual targets. *PLoS Biol, 2*(6), e176. doi: 10.1371/journal.pbio.0020176

Makeig, S., Kothe, C., Mullen, T., Bigdely Shamlo, N., Zhang, Z., & Kreutz-Delgado, K. (2012). Evolving Signal Processing for Brain-Computer Interfaces. *Proceedings of the IEEE, 100*(Special Centennial Issue), 1567-1584. doi: 10.1109/JPROC.2012.2185009

Makeig, S., Westerfield, M., Jung, T. P., Covington, J., Townsend, J., Sejnowski, T. J., & Courchesne, E. (1999). Functionally independent components of the late positive event-related potential during visual spatial attention. *J Neurosci, 19*(7), 2665-2680.

Malone, S. M., Luciana, M., Wilson, S., Sparks, J. C., Hunt, R. H., Thomas, K. M., & Iacono, W. G. (2014). Adolescent drinking and motivated decision-making: a cotwin-control investigation with monozygotic twins. *Behav Genet, 44*(4), 407-418. doi: 10.1007/s10519-014-9651-0

Marquardt, L., Eichele, H., Lundervold, A. J., Haavik, J., & Eichele, T. (2018). Event-Related-Potential (ERP) Correlates of Performance Monitoring in Adults With Attention-Deficit Hyperactivity Disorder (ADHD). *Front Psychol, 9*, 485. doi: 10.3389/fpsyg.2018.00485

Masaki, H., Murphy, T. I., Kamijo, K., Yamazaki, K., & Sommer, W. (2012). Foreshadowing of performance accuracy by event-related potentials: evidence from a minimal-conflict task. *PLoS One, 7*(5), e38006. doi: 10.1371/journal.pone.0038006

McLoughlin, G., Albrecht, B., Banaschewski, T., Rothenberger, A., Brandeis, D., Asherson, P., & Kuntsi, J. (2009). Performance monitoring is altered in adult ADHD: a familial event-related potential investigation. *Neuropsychologia, 47*(14), 3134-3142. doi: 10.1016/j.neuropsychologia.2009.07.013

McLoughlin, G., Makeig, S., & Tsuang, M. T. (2014). In search of biomarkers in psychiatry: EEG-based measures of brain function. *Am J Med Genet B Neuropsychiatr Genet, 165B*(2), 111-121. doi: 10.1002/ajmg.b.32208

McLoughlin, G., Palmer, J. A., Rijsdijk, F., & Makeig, S. (2013). Genetic Overlap between Evoked Frontocentral Theta-Band Phase Variability, Reaction Time Variability, and Attention-Deficit/Hyperactivity Disorder Symptoms in a Twin Study. *Biol Psychiatry*. doi: 10.1016/j.biopsych.2013.07.020

Meckler, C., Carbonnell, L., Hasbroucq, T., Burle, B., & Vidal, F. (2013). To err or to guess: an ERP study on the source of errors. *Psychophysiology, 50*(5), 415-421. doi: 10.1111/psyp.12020

Meyer, A., Bress, J. N., & Proudfit, G. H. (2014). Psychometric properties of the error-related negativity in children and adolescents. *Psychophysiology, 51*(7), 602-610. doi: 10.1111/psyp.12208

Mullane, J. C., Corkum, P. V., Klein, R. M., & McLaughlin, E. (2009). Interference control in children with and without ADHD: a systematic review of Flanker and Simon task performance. *Child Neuropsychol, 15*(4), 321-342. doi: 10.1080/09297040802348028

Mullen, T. R., Kothe, C. A., Chi, Y. M., Ojeda, A., Kerth, T., Makeig, S., . . . Cauwenberghs, G. (2015). Real-Time Neuroimaging and Cognitive Monitoring Using Wearable Dry EEG. *IEEE Trans Biomed Eng, 62*(11), 2553-2567. doi: 10.1109/TBME.2015.2481482

Nachev, P., Kennard, C., & Husain, M. (2008). Functional role of the supplementary and pre-supplementary motor areas. *Nat Rev Neurosci, 9*(11), 856-869. doi: 10.1038/nrn2478

Nieuwenhuis, S., Ridderinkhof, K. R., Blom, J., Band, G. P., & Kok, A. (2001). Error-related brain potentials are differentially related to awareness of response errors: evidence from an antisaccade task. *Psychophysiology, 38*(5), 752-760.

O'Connell, R. G., Dockree, P. M., Robertson, I. H., Bellgrove, M. A., Foxe, J. J., & Kelly, S. P. (2009). Uncovering the neural signature of lapsing attention: electrophysiological signals predict errors up to 20 s before they occur. *J Neurosci, 29*(26), 8604-8611. doi: 10.1523/JNEUROSCI.5967-08.2009

Obeso, I., Cho, S. S., Antonelli, F., Houle, S., Jahanshahi, M., Ko, J. H., & Strafella, A. P. (2013). Stimulation of the pre-SMA influences cerebral blood flow in frontal areas involved with inhibitory control of action. *Brain Stimul, 6*(5), 769-776. doi: 10.1016/j.brs.2013.02.002

Onton, J., Westerfield, M., Townsend, J., & Makeig, S. (2006). Imaging human EEG dynamics using independent component analysis. *Neurosci Biobehav Rev, 30*(6), 808-822. doi: 10.1016/j.neubiorev.2006.06.007

Overbeek, T. J. M., Nieuwenhuis, S., & Ridderinkhof, K. R. (2005). Dissociable components of error processing - On the functional significance of the Pe Vis-a-vis the ERN/Ne. *Journal of Psychophysiology, 19*(4), 319-329. doi: 10.1027/0269-8803.19.4.319

Palmer, J., Kreutz-Delgado, K., & Makeig, S. (2006). An Independent Component Analysis Mixture Model with Adaptive Source Densities. *Journal of Machine Learning Research*.

Palmer, J. A., Kreutz-Delgado, K., Rao, B. D., & Makeig, S. (2007). Modeling and estimation of dependent subspaces with non-radially symmetric and skewed densities. *Independent Component Analysis and Signal Separation, Proceedings, 4666*, 97-+.

Pape, A. A., & Siegel, M. (2016). Motor cortex activity predicts response alternation during sensorimotor decisions. *Nat Commun, 7*, 13098. doi: 10.1038/ncomms13098

Perri, R. L., Berchicci, M., Lucci, G., Spinelli, D., & Di Russo, F. (2015). Why do we make mistakes? Neurocognitive processes during the preparation-perception-action cycle and error-detection. *Neuroimage, 113*, 320-328. doi: 10.1016/j.neuroimage.2015.03.040

Perri, R. L., Berchicci, M., Spinelli, D., & Di Russo, F. (2014). Individual differences in response speed and accuracy are associated to specific brain activities of two interacting systems. *Front Behav Neurosci, 8*, 251. doi: 10.3389/fnbeh.2014.00251

Piazza, C., Cantiani, C., Akalin-Acar, Z., Miyakoshi, M., Benasich, A. A., Reni, G., . . . Makeig, S. (2016). ICA-derived cortical responses indexing rapid multi-feature auditory processing in six-month-old infants. *Neuroimage, 133*, 75-87. doi: 10.1016/j.neuroimage.2016.02.060

Pinheiro, J. C., & Bates, D. M. (2000). *Mixed-effects models in S and S-PLUS*. New York: Springer.

Pontifex, M. B., Raine, L. B., Johnson, C. R., Chaddock, L., Voss, M. W., Cohen, N. J., . . . Hillman, C. H. (2011). Cardiorespiratory fitness and the flexible modulation of cognitive control in preadolescent children. *J Cogn Neurosci, 23*(6), 1332-1345. doi: 10.1162/jocn.2010.21528

Pontifex, M. B., Saliba, B. J., Raine, L. B., Picchietti, D. L., & Hillman, C. H. (2013). Exercise improves behavioral, neurocognitive, and scholastic performance in children with attention-deficit/hyperactivity disorder. *J Pediatr, 162*(3), 543-551. doi: 10.1016/j.jpeds.2012.08.036

Potts, G., Liotti, M., Tucker, D. M., & Posner, M. I. (1996). Frontal and inferior temporal cortical activity in visual target detection: evidence from high spatially sampled event-related potentials. *Brain Topogr, 9*(1), 12.

Rapela, J., Gramann, K., Westerfield, M., Townsend, J., & Makeig, S. (2012). Brain oscillations in switching vs. focusing audio-visual attention. *Conf Proc IEEE Eng Med Biol Soc, 2012*, 352-355. doi: 10.1109/EMBC.2012.6345941

Reich, W. (2000). Diagnostic interview for children and adolescents (DICA). *J Am Acad Child Adolesc Psychiatry, 39*(1), 59-66. doi: 10.1097/00004583-200001000-00017

Ridderinkhof, K. R., Nieuwenhuis, S., & Bashore, T. R. (2003). Errors are foreshadowed in brain potentials associated with action monitoring in cingulate cortex in humans. *Neurosci Lett, 348*(1), 1-4.

Ridderinkhof, K. R., Ullsperger, M., Crone, E. A., & Nieuwenhuis, S. (2004). The role of the medial frontal cortex in cognitive control. *Science, 306*(5695), 443-447. doi: 10.1126/science.1100301

Roger, C., Nunez Castellar, E., Pourtois, G., & Fias, W. (2014). Changing your mind before it is too late: the electrophysiological correlates of online error correction during response selection. *Psychophysiology, 51*(8), 746-760. doi: 10.1111/psyp.12224

Roman, R., Brazdil, M., Jurak, P., Rektor, I., & Kukleta, M. (2005). Intracerebral P3-like waveforms and the length of the stimulus-response interval in a visual oddball paradigm. *Clin Neurophysiol, 116*(1), 160-171. doi: 10.1016/j.clinph.2004.07.016

Rousselet, G. A., Husk, J. S., Pernet, C. R., Gaspar, C. M., Bennett, P. J., & Sekuler, A. B. (2009). Age-related delay in information accrual for faces: evidence from a parametric, single-trial EEG approach. *BMC Neurosci, 10*, 114. doi: 10.1186/1471-2202-10-114

Salisbury, D. F., Rutherford, B., Shenton, M. E., & McCarley, R. W. (2001). Button-pressing affects P300 amplitude and scalp topography. *Clin Neurophysiol, 112*(9), 1676-1684.

Shrout, P. E., & Bolger, N. (2002). Mediation in experimental and nonexperimental studies: new procedures and recommendations. *Psychol Methods, 7*(4), 422-445.

Silverman, M. H., Krueger, R. F., Iacono, W. G., Malone, S. M., Hunt, R. H., & Thomas, K. M. (2014). Quantifying familial influences on brain activation during the monetary incentive delay task: an adolescent monozygotic twin study. *Biol Psychol, 103*, 7-14. doi: 10.1016/j.biopsycho.2014.07.016

Smith, N. J. (2011). *Scaling up psycholinguistics.* (Cognitive Science Doctoral thesis), University of California San Diego. Retrieved from https://escholarship.org/uc/item/9hh0x7tq

Smith, N. J., & Kutas, M. (2015a). Regression-based estimation of ERP waveforms: I. The rERP framework. *Psychophysiology, 52*(2), 157-168. doi: 10.1111/psyp.12317

Smith, N. J., & Kutas, M. (2015b). Regression-based estimation of ERP waveforms: II. Nonlinear effects, overlap correction, and practical considerations. *Psychophysiology, 52*(2), 169-181. doi: 10.1111/psyp.12320

Smulders, F. T. Y., & Miller, J. O. (2011). The Lateralized Readiness Potential. In E. S. Kappenman & S. J. Luck (Eds.), *The Oxford Handbook of Event-Related Potential Components*: Oxford University Press.

Sonuga-Barke, E. J., & Castellanos, F. X. (2007). Spontaneous attentional fluctuations in impaired states and pathological conditions: a neurobiological hypothesis. *Neurosci Biobehav Rev, 31*(7), 977-986. doi: 10.1016/j.neubiorev.2007.02.005

Spieser, L., van den Wildenberg, W., Hasbroucq, T., Ridderinkhof, K. R., & Burle, B. (2015). Controlling your impulses: electrical stimulation of the human supplementary motor complex prevents impulsive errors. *J Neurosci, 35*(7), 3010-3015. doi: 10.1523/JNEUROSCI.1642-14.2015

Swensen, A., Birnbaum, H. G., Ben Hamadi, R., Greenberg, P., Cremieux, P. Y., & Secnik, K. (2004). Incidence and costs of accidents among attention-deficit/hyperactivity disorder patients. *J Adolesc Health, 35*(4), 346 e341-349.

Torpey, D. C., Hajcak, G., Kim, J., Kujawa, A., & Klein, D. N. (2012). Electrocortical and behavioral measures of response monitoring in young children during a Go/No-Go task. *Dev Psychobiol, 54*(2), 139-150. doi: 10.1002/dev.20590

Tsai, A. C., Jung, T. P., Chien, V. S., Savostyanov, A. N., & Makeig, S. (2014). Cortical surface alignment in multi-subject spatiotemporal independent EEG source imaging. *Neuroimage, 87*, 297-310. doi: 10.1016/j.neuroimage.2013.09.045

Tzourio-Mazoyer, N., Landeau, B., Papathanassiou, D., Crivello, F., Etard, O., Delcroix, N., . . . Joliot, M. (2002). Automated anatomical labeling of activations in SPM using a macroscopic anatomical parcellation of the MNI MRI single-subject brain. *Neuroimage, 15*(1), 273-289. doi: 10.1006/nimg.2001.0978

Udupa, K., & Chen, R. (2013). Central motor conduction time. *Handb Clin Neurol, 116*, 375-386. doi: 10.1016/B978-0-444-53497-2.00031-0

Vaa, T. (2014). ADHD and relative risk of accidents in road traffic: a meta-analysis. *Accid Anal Prev, 62*, 415-425. doi: 10.1016/j.aap.2013.10.003

Watanabe, T., Hanajima, R., Shirota, Y., Tsutsumi, R., Shimizu, T., Hayashi, T., . . . Konishi, S. (2015). Effects of rTMS of pre-supplementary motor area on fronto basal ganglia network activity during stop-signal task. *J Neurosci, 35*(12), 4813-4823. doi: 10.1523/JNEUROSCI.3761-14.2015

Weissman, D. H., Roberts, K. C., Visscher, K. M., & Woldorff, M. G. (2006). The neural bases of momentary lapses in attention. *Nat Neurosci, 9*(7), 971-978. doi: 10.1038/nn1727

Wessel, J. R. (2012). Error awareness and the error-related negativity: evaluating the first decade of evidence. *Front Hum Neurosci, 6*, 88. doi: 10.3389/fnhum.2012.00088

Wessel, J. R., & Aron, A. R. (2015). It's not too late: the onset of the frontocentral P3 indexes successful response inhibition in the stop-signal paradigm. *Psychophysiology, 52*(4), 472-480. doi: 10.1111/psyp.12374

Wilson, S., Malone, S. M., Thomas, K. M., & Iacono, W. G. (2015). Adolescent drinking and brain morphometry: A co-twin control analysis. *Dev Cogn Neurosci, 16*, 130-138. doi: 10.1016/j.dcn.2015.07.005

Winkler, I., Debener, S., Muller, K. R., & Tangermann, M. (2015). On the influence of high-pass filtering on ICA-based artifact reduction in EEG-ERP. *Conf Proc IEEE Eng Med Biol Soc, 2015*, 4101-4105. doi: 10.1109/EMBC.2015.7319296

Woldorff, M. G. (1993). Distortion of ERP averages due to overlap from temporally adjacent ERPs: analysis and correction. *Psychophysiology, 30*(1), 98-119.

Yamane, S., Nambu, I., & Wada, Y. (2014). Predicting occurrence of errors during a Go/No-Go task from EEG signals using Support Vector Machine. *Conf Proc IEEE Eng Med Biol Soc, 2014*, 4944-4947. doi: 10.1109/EMBC.2014.6944733

Yordanova, J., Albrecht, B., Uebel, H., Kirov, R., Banaschewski, T., Rothenberger, A., & Kolev, V. (2011). Independent oscillatory patterns determine performance fluctuations in children with attention deficit/hyperactivity disorder. *Brain, 134*(Pt 6), 1740-1750. doi: 10.1093/brain/awr107